### Title

GIV•Kindlin Interaction Is Required for Kindlin-Mediated Integrin Recognition and Activation




### Journal

iScience, 23(6)

### ISSN

2589-0042



### Authors

Rohena, Cristina

Kalogriopoulos, Nicholas

Rajapakse, Navin

et al.



### Publication Date

2020-06-01

### DOI

10.1016/j.isci.2020.101209

iScience

CellPress
OPEN ACCESS

Article

# GIV●Kindlin Interaction Is Required for Kindlin-Mediated Integrin Recognition and Activation

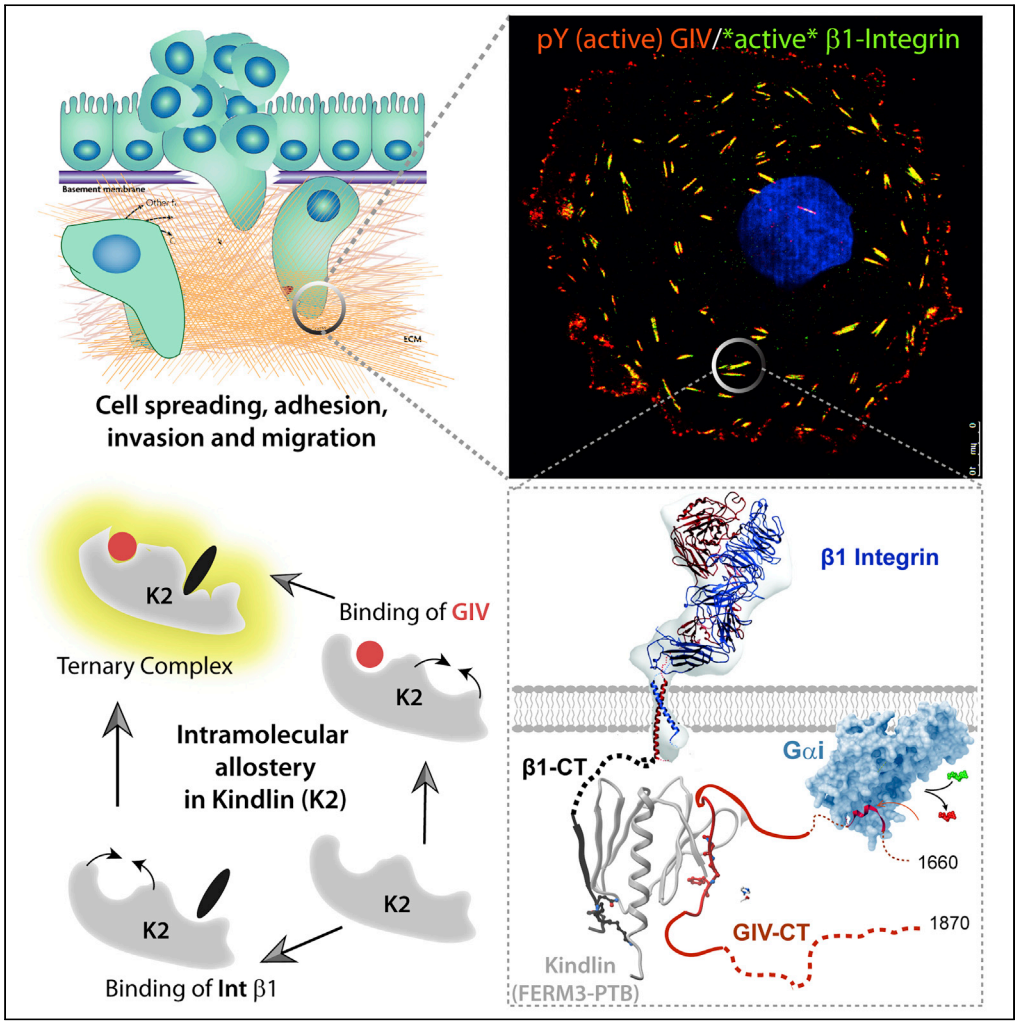


Cristina Rohena, Nicholas Kalogriopoulos, Navin Rajapakse, ..., Jailal Ablack, Debashis Sahoo, Pradipta Ghosh

prghosh@ucsd.edu

## HIGHLIGHTS

GIV and Kindlin (K2), two integrin adaptors that promote metastasis, bind each other

Binding of GIV or integrin to K2 allosterically enhances GIV•K2•integrin complexes

Binding is required for the maximal recruitment of GIV and K2 to active integrins

Binding facilitates integrin clustering, activation, tumor cell adhesion, invasion

Rohena et al., iScience 23, 101209
June 26, 2020 
https://doi.org/10.1016/j.isci.2020.101209

iScience

CellPress
OPEN ACCESS

Article

# GIV●Kindlin Interaction Is Required for Kindlin-Mediated Integrin Recognition and Activation

Cristina Rohena,[1,7] Nicholas Kalogriopoulos,[1,2,7] Navin Rajapakse,[2] Suchismita Roy,[2] Inmaculada Lopez-Sanchez,[1] Jailal Ablack,[1] Debashis Sahoo,[3,4,5] and Pradipta Ghosh[1,2,5,6,8,*]

## SUMMARY

**Cells perceive and respond to the extracellular matrix via integrin receptors; their dysregulation has been implicated in inflammation and cancer metastasis. Here we show that a guanine nucleotide-exchange modulator of trimeric-GTPase Gαi, GIV (a.k.a Girdin), directly binds the integrin adaptor Kindlin-2. A non-canonical short linear motif within the C terminus of GIV binds Kindlin-2-FERM3 domain at a site that is distinct from the binding site for the canonical NPxY motif on the -integrin tail. Binding of GIV to Kindlin-2 allosterically enhances Kindlin-2's affinity for β1-integrin. Consequently, integrin activation and clustering are maximized, which augments cell adhesion, spreading, and invasion. Findings elucidate how the GIV●Kindlin-2 complex has a 2-fold impact: it allosterically synergizes integrin activation and enables β1-integrins to indirectly access and modulate trimeric GTPases via the complex. Furthermore, Cox proportional-hazard models on tumor transcriptomics provide trans-scale evidence of synergistic interactions between GIV●Kindlin-2●β1-integrin on time to progression to metastasis.**

## INTRODUCTION

Cell adhesion to extracellular matrix (ECM) proteins and to neighboring cells is essential for multicellular organisms. Cells perceive and respond to the composition and stiffness of the ECM through mechanotransduction via integrin class of receptors. As key regulators of cell fate, e.g., survival, proliferation, and migration, integrins are essential for embryonic development, and their aberrant signaling fuels numerous diseases, including inflammation, tumor growth, chemoresistance, and metastasis.

Several adaptor proteins transduce integrin signals by directly binding to the cytoplasmic tails of β-integrins (Legate and Fassler, 2009). Among them, only talin and kindlin are known to be indispensable for integrin activation (Theodosiou et al., 2016; Calderwood et al., 2013). The phosphotyrosine-binding (PTB)-like module in talin's FERM3 domain binds to the membrane-proximal NPxY motif of β-integrin cytoplasmic tails. Kindlin is also a FERM3 domain-containing protein that binds to the membrane distal NPxY motif on integrin tails. Structural, biochemical, and mutational approaches revealed that talin-mediated integrin activation results in conformational changes in the receptor's transmembrane helix (Lau et al., 2008a, 2008b) and how such activation requires first the reversal of an intramolecular autoinhibitory contact within talin, between its FERM3-PTB and its rod domains (Vinogradova et al., 2002; Wegener et al., 2007; Goksoy et al., 2008; Garcia-Alvarez et al., 2003). By contrast, kindlin does not have the ability to directly alter the conformation of the integrin transmembrane helix and instead augments integrin activation in cooperativity with talin (Bledzka et al., 2012), without which the conformational shift of integrins from the low- to high-affinity state cannot occur and maximal activation is not possible (Campbell and Humphries, 2011; Calderwood et al., 2013).

Regarding mechanistic insights into how adaptor binding translates to integrin activation, gathering evidence suggests that activation occurs by fine-tuning the affinity of talin and kindlin for integrins. Talin's affinity for integrins, for example, can be regulated either through proteolytic relief of auto-inhibition or through membrane recruitment and molecular allostery upon direct binding of phosphoinositides to the FERM3 domain (Moore et al., 2012; Ye et al., 2016; Lagarrigue et al., 2016; Lee et al., 2009; Han et al., 2006). In the case of kindlin, however, despite the discovery of numerous interacting partners (Theodosiou

[1]Department of Medicine, University of California San Diego, 9500 Gilman Drive (MC 0651), George E. Palade Bldg, Rm 239, La Jolla, CA 92093, USA

[2]Department of Cellular and Molecular Medicine, University of California San Diego, CA 92093, USA

[3]Department of Pediatrics, University of California San Diego, CA 92093, USA

[4]Department of Computer Science and Engineering, Jacob's School of Engineering, University of California San Diego, CA 92093, USA

[5]Rebecca and John Moore Comprehensive Cancer Center, University of California San Diego, CA 92093, USA

[6]Veterans Affairs Medical Center, 3350 La Jolla Village Drive, San Diego, CA 92161, USA

[7]These authors contributed equally

[8]Lead Contact

*Correspondence: prghosh@ucsd.edu

https://doi.org/10.1016/j.isci.2020.101209

et al., 2016; Fukuda et al., 2014; Bottcher et al., 2017) that coordinate the activation of focal adhesion kinase (FAK), Rac1, and the Arp2/3 complex within the so-called adhesome complex (Theodosiou et al., 2016; Bottcher et al., 2017; Zaidel-Bar et al., 2007; Winograd-Katz et al., 2014), who or what may fine-tune the affinity of kindlin for integrins remains unknown and whether such fine-tuning enhances initial integrin activation, clustering, and adhesion strengthening remains elusive.

Besides talin and kindlin, we (Lopez-Sanchez et al., 2015) and others (Leyme et al., 2015, 2016) have recently reported that exposing cells to ECM also triggers the tyrosine phosphorylation of another adaptor protein, GIV, and that focal adhesions (FAs) serve as the major hubs for tyr-based mechanochemical signaling via GIV. GIV is a guanine nucleotide exchange factor (GEF) for trimeric GTPase, Gi (Garcia-Marcos et al., 2009; Kalogriopoulos et al., 2019), and is an actin remodeler (Enomoto et al., 2005). Published work has shown that GIV (and Gαi via GIV) interacts exclusively with ligand-activated β1-integrins and GIV's GEF function is essential for the subsequent activation of Gαi in response to stimuli (Leyme et al., 2015; Lopez-Sanchez et al., 2015). GIV-dependent Gi activation and release of "free" Gβγ-heterodimer modulates multiple downstream signals including FAK activation, remodeling of the actin cytoskeleton, and Rac1 and PI3K-dependent signaling, resulting in enhanced haptotaxis and invasion (Leyme et al., 2015). These signals and cellular phenotypes are further reinforced via a forward-feedback loop in which activated FAK phosphorylates GIV and that such phosphorylation further enhances PI3K-Akt signaling, the integrity of FAs, and cell adhesion and motility (Leyme et al., 2016; Lopez-Sanchez et al., 2015). Spatially restricted signaling via tyrosine phosphorylated GIV at the FAs is enhanced during cancer metastasis (Midde et al., 2018). Despite these insights, how GIV binds integrins remained unclear; because they co-immunoprecipitated from cells, but recombinant GIV and β-integrin cytoplasmic tails did not interact *in vitro*, the interaction was assumed to be indirect (Lopez-Sanchez et al., 2015).

We set out to investigate how GIV gains access to β-integrin cytoplasmic tails but unexpectedly stumbled upon an intermolecular interplay between GIV, kindlin, and β1-integrin. Findings help answer some of the fundamental unanswered questions, e.g., how GIV may bind integrins to impact downstream signaling and how kindlin may bring about maximal integrin activation; they also provide mechanistic insights into how cooperativity between the two adaptors may be essential for both.

## RESULTS AND DISCUSSION

### GIV Interacts with Ligand-Activated β1-Integrins Indirectly via Kindlin-2

Prior work had shown that GIV indirectly associates with β1-integrins early (within minutes) during cell adhesion and localizes to nascent focal adhesions (FAs) at the cell periphery well before integrins cluster and FAs mature. Because integrin activation and clustering, two of the earliest steps of cell adhesion, require sequential recruitment of the adaptor proteins talin, then kindlin, and finally, tensin (Bachir et al., 2014; Calderwood et al., 2013; Montanez et al., 2008), we hypothesized that GIV may interact with one or more of these adaptors. To test this hypothesis, we carried out pull-down studies using recombinant GST-tagged integrin-binding FERM3/PTB modules of the key adaptor proteins (Talin, Kindlin, and Tensin) and His-tagged C-terminal fragment of GIV (GIV-CT; ~ 210 aa). To avoid common problems encountered when generating protein fragments (misfolding, degradation, unforeseen/undesired mutations, all leading to non-functional proteins, we refrained from creating new constructs and instead curated previously published constructs that were validated in various biochemical or crystallography studies to interrogate integrin biology and sequenced them to confirm accuracy (see Methods). As for GIV-CT, it has previously been shown to bind cytoplasmic tails of multiple growth factor receptors (Lin et al., 2014), G proteins (Garcia-Marcos et al., 2009), FAK (Lopez-Sanchez et al., 2015), and p85α-PI3K (Lin et al., 2011); prior work also showed that GIV-CT is sufficient to trigger cancer cell invasion (Ma et al., 2015a; Midde et al., 2015). Among the three Kindlins (K1–3), we chose to study kindlin-2 (K2) because, unlike K1 and K3, which are expressed in restricted cells/tissues (i.e., epithelial and hematopoietic system, which express GIV at very low levels [Enomoto et al., 2005]), K2 is expressed ubiquitously (Rognoni et al., 2016). We found that GIV specifically bound the FERM3-PTB module of K2 and to the PTB module of tensin but not to the FERM2-PTB module of talin (Figure 1A). Because GIV was previously shown to accumulate early during cell adhesion within nascent FAs at the cell periphery (Lopez-Sanchez et al., 2015), where K2 is known to exist at a 1:1 ratio with β1-integrins (Sun et al., 2014), and tensin on the other hand is typically enriched later in FAs during the course of tension-dependent maturation (Zaidel-Bar et al., 2004), we chose to further dissect the nature and relevance of the GIV●K2 interaction. Full-length GIV (from cell lysates) could also bind GST-K2, but little or no binding was observed with GST-β-integrin tails (Figure 1B). We also confirmed that the reverse was also true, in that,

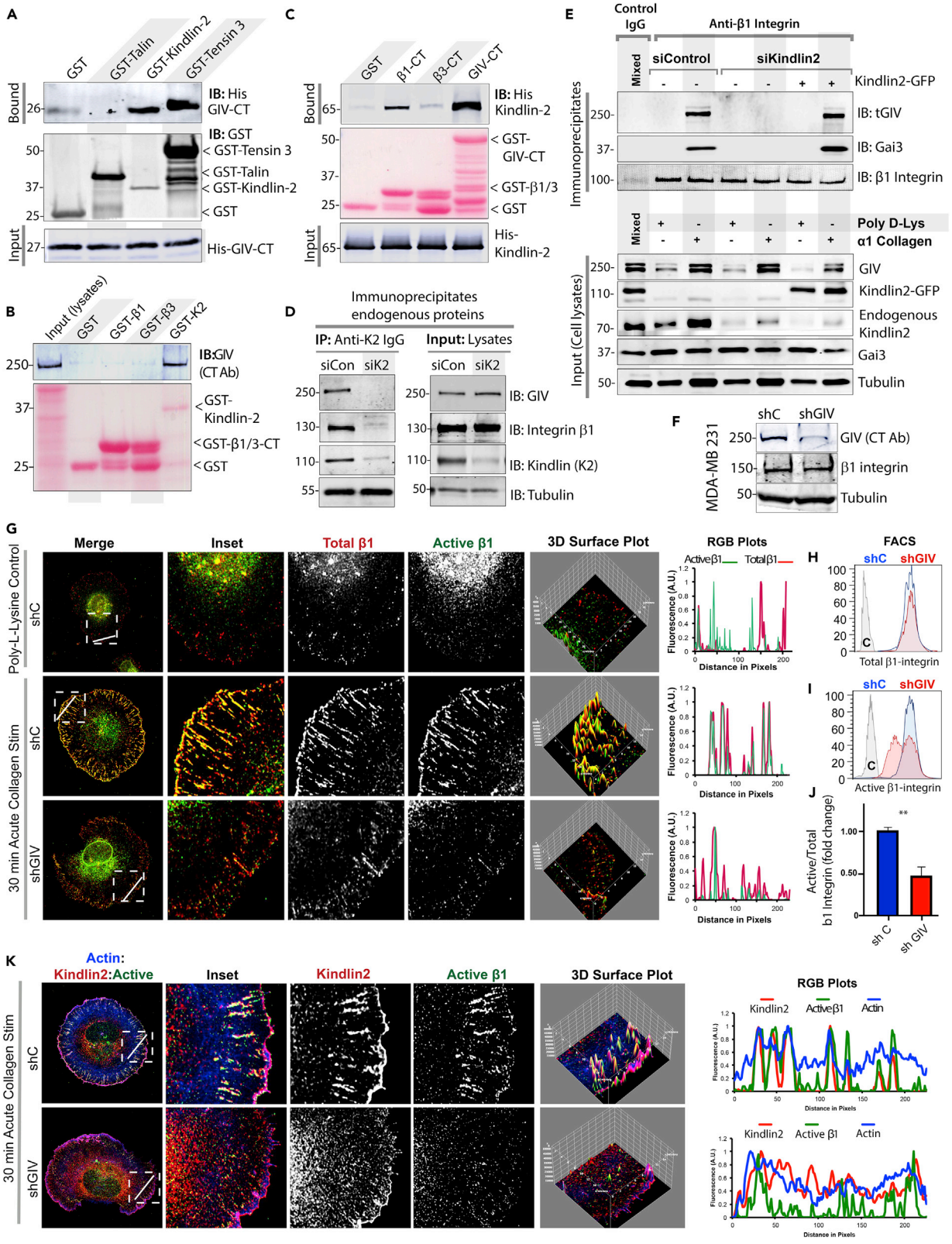
A
GST
GST-Talin
GST-Kindlin-2
GST-Tensin 3
Bound
Input
IB: His GIV-CT
IB: GST
< GST-Tensin 3
< GST-Talin
< GST-Kindlin-2
< GST
His-GIV-CT
B
Input (lysates)
GST
GST-β1
GST-β3
GST-K2
IB:GIV (CT Ab)
< GST-Kindlin-2
< GST-β1/3-CT
< GST
C
GST
β1-CT
β3-CT
GIV-CT
IB: His Kindlin-2
< GST-GIV-CT
< GST-β1/3
< GST
His-Kindlin-2
D
Immunoprecipitates endogenous proteins
IP: Anti-K2 IgG
Input: Lysates
siCon
siK2
IB: GIV
IB: Integrin β1
IB: Kindlin (K2)
IB: Tubulin
E
Control IgG
Anti-β1 Integrin
Mixed
siControl
siKindlin2
Kindlin2-GFP
Immunoprecipitates
IB: tGIV
IB: Gai3
IB: β1 Integrin
Poly D-Lys
α1 Collagen
Input (Cell lysates)
GIV
Kindlin2-GFP
Endogenous Kindlin2
Gai3
Tubulin
F
shC
shGIV
MDA-MB 231
GIV (CT Ab)
β1 integrin
Tubulin
G
Merge
Inset
Total β1
Active β1
3D Surface Plot
RGB Plots
Poly-L-Lysine Control
30 min Acute Collagen Stim
shC
shGIV
Fluorescence (A.U.)
Distance in Pixels
H
FACS
shC
shGIV
Total β1-integrin
I
Active β1-integrin
J
Active/Total b1 Integrin (fold change)
sh C
sh GIV
K
Actin:
Kindlin2:Active
Kindlin2
Actin

**Figure 1. GIV Binds Kindlin-2 and Is Required for kindlin Recruitment to Integrin β1 at Focal Adhesions and for Maximal Integrin Activation**

(A) GST pull-down assays were performed using equal aliquots of recombinant His-GIV-CT (aa 1,660–1,870; ~3 μg) and various FERM3/PTB fragments of GST-tagged adaptor proteins known to bind integrin-β receptors. Bound His-GIV-CT and various GST ligands were visualized by immunoblotting using an anti-His mAb and an anti-GST pAb, respectively.

(B) Equal aliquots of lysates of MDA-MB-231 cells were used as source for full-length endogenous GIV in GST pull-down assays with GST-Kindlin 2 (K2), GST-β1, or GST-β3 proteins. Bound GIV was visualized by immunoblotting using anti-GIV-CT rabbit polyAb. Equal loading of GST proteins was confirmed by Ponceau S staining.

(C) GST pull-down assays were performed using recombinant His-Kindlin 2 (6xHis-SUMO-Kindlin2Δ [Li et al., 2017]) and GST-GIV-CT (aa 1,623–1,870). Bound kindlin-2 was analyzed by immunoblotting with anti-His mAb. GST proteins were visualized by Ponceau S staining. GST-β1 and GST-β3 integrin tails were used as positive and negative controls, respectively. See also Figure S1A for bar graphs displaying quantification.

(D) Immunoprecipitation studies with anti-Kindlin2 (K2) antibody on lysates of control (siC) or kindlin-2-depleted (by siKindlin-2) HeLa cells. Immune complexes were analyzed for GIV, Integrin- β1, and Kindlin2 by immunoblotting (IB).

(E) Control (siC) or kindlin-2-depleted (by siKindlin-2) HeLa cells reconstituted or not with GFP-Kindlin-2, grown on poly-D-Lysine-coated surface, were stimulated (+) or not (−) by plating on collagen-coated surface for 30 min before lysis. Equal aliquots of lysates (Input cell lysates) were subjected to immunoprecipitation using anti-β1-integrin antibody. Immune complexes were analyzed for total (t)GIV, β1-integrin, and Gαi3 by immunoblotting. The differences in levels of tGIV in input lysates likely reflects differential extraction by Triton X-100 in cells plated on poly-D-Lysine versus collagen-plated coverslips.

(F) MDA-MB-231 cells depleted (shGIV) or not (shC) of GIV by shRNA were analyzed for GIV and tubulin by immunoblotting with respective antibodies.

(G) Cell lines in (F) were grown on poly-D-Lysine-coated surface and were stimulated by plating on collagen-coated cover slips for 30 min, fixed, and stained for active β1-integrin (green; using a conformational specific antibody, clone 9EG7), phalloidin (blue; actin), and total β1-integrin (red) and analyzed by confocal microscopy. Representative deconvolved images are shown. Insets were analyzed by rendering 3D surface plots, and line scans were taken to generate RGB plots using ImageJ.

(H and I) FACS histograms (H, I) of cells in (F) showing cell-surface expression of total (H) and active β1 (I), as measured by 9EG7 staining. C, IgG negative control.

(J) Bar graphs showing fold change in the proportion of activation of β1-integrin (active/total) in (H) and (I). Data are represented as mean ± SEM (n = 3); **p=<0.01.

(K) Cells in (G) were fixed and stained for active β1-integrin (green; using a conformational specific antibody, clone 9EG7), phalloidin (blue; actin), and K2 (red) and analyzed by confocal microscopy. Representative deconvolved images are shown. Insets were analyzed by rendering 3D surface plots, and line scans were taken to generate RGB plots using ImageJ.

when GST-GIV-CT was immobilized on glutathione beads, it could directly bind His-K2 (Figures 1C and S1A); to our surprise, in this assay, K2 bound GIV-CT much better than it bound our positive control (GST-β1-CT). Because one prior study (Leyme et al., 2015) claimed the existence of a possible weak, but direct, interaction between GIV's N terminus (GIV-NT; aa 1–256) and the cytoplasmic tail of β1-integrin, we compared side by side the ability of the N- and C-terminal fragments to bind GST-β1-CT and K2. We found that neither the C nor the N terminus of GIV bound the cytoplasmic tail of integrin β1 to any appreciable degree when compared with the binding of GIV-CT to K2 (Figure S1B). Furthermore, co-immunoprecipitation studies confirmed that the interaction we observe between tagged recombinant proteins *in vitro* occurs also between full-length endogenous GIV and kindlin2 proteins in cells (Figure 1D). These findings demonstrate that the C terminus of GIV directly and specifically binds the integrin-adaptor K2 and suggest that previously reported interactions of GIV and G protein, Gi with ligand-activated β1-integrin in cells are likely to be indirect (via K2). Indeed, we confirmed this to be true, because neither GIV nor Gαi was detectable within β1-integrin-bound complexes when we depleted HeLa cells of endogenous K2 but they were readily detectable when a small interfering RNA (siRNA)-resistant GFP-tagged K2 was exogenously expressed in these cells (Figure 1E). Although it is possible that impaired formation of focal adhesions in cells without kindlin-2 may preclude the GIV●β1-integrin interaction, together with the biochemical evidence of direct interaction and interactions observed in cells, our findings indicate that GIV interacts with ligand-activated β1-integrins indirectly via kindlin-2.

## GIV Is Required for Integrin Activation, Formation of β1-integrin●Kindlin Complexes at Focal Adhesions

Because K2 is believed to be indispensable for integrin activation (Theodosiou et al., 2016; Calderwood et al., 2013), next we analyzed if GIV, which is co-recruited with K2 is also required for the same. To this end, we used control and GIV-depleted MDA-MB-231 breast cancer cells, a model system that was previously used by others to implicate GIV's role in integrin-dependent downstream activation of the PI3K-Akt and RhoA pathways (Leyme et al., 2015), stimulated them by plating on collagen-coated cover slips and stained them with a previously validated conformation-sensitive rat anti-CD29 9EG7 antibody. We found that cells without GIV had significantly reduced integrin activation, both within nascent FAs in the cell periphery and within mature FAs (Figure 1G), indicating that much like K2, GIV is also required for β1-integrin activation. Flow cytometry studies using the same antibody further confirmed that activation of β1-integrins

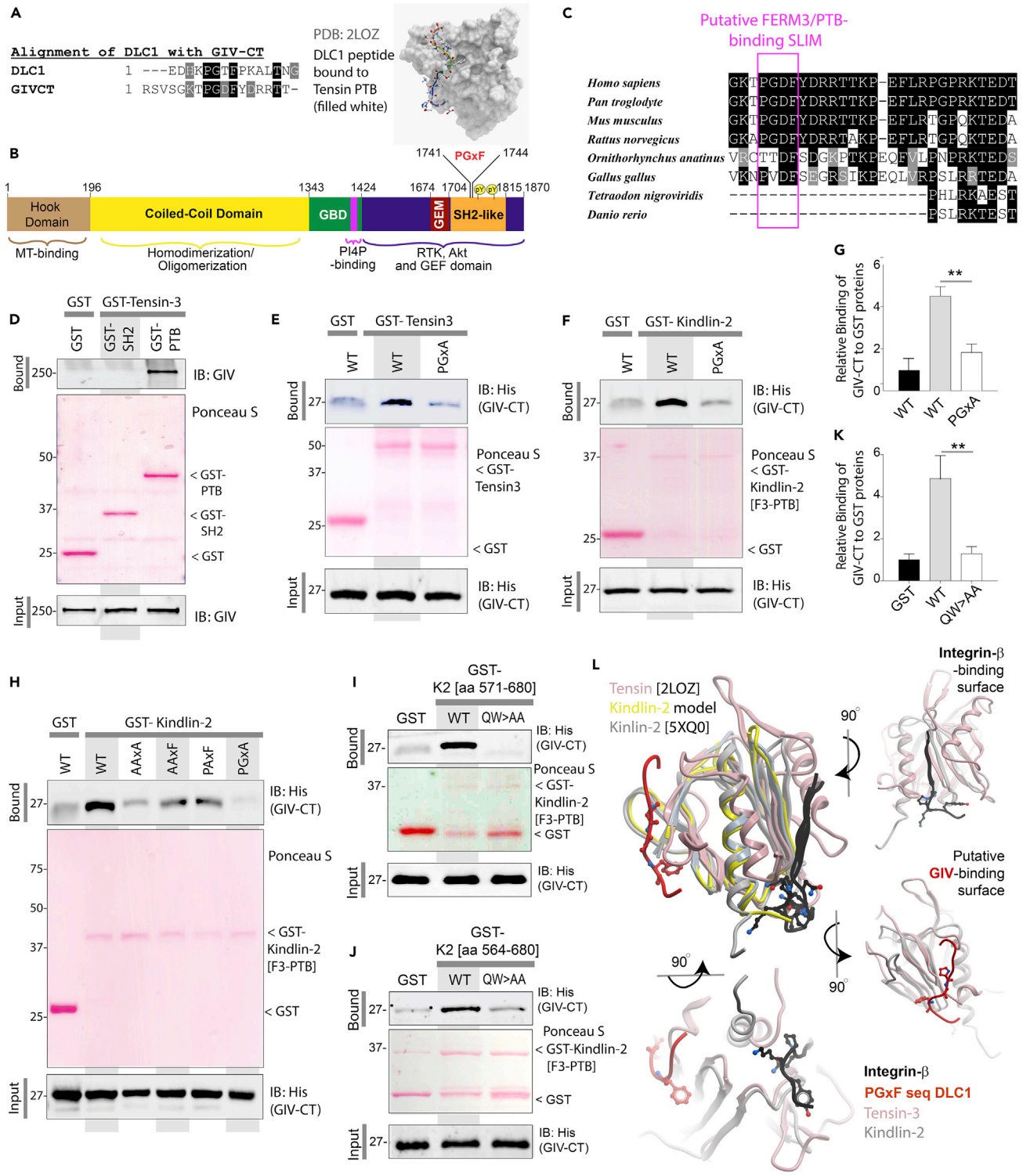


**Figure 2. Identification and Validation of a Short Linear Motif (SLIM) in GIV that Directly Binds the FERM3(F3)-PTB Module in Kindlin-2 (K2)**

(A) Sequence alignment between the C terminus of GIV and DLC1 (which binds Tensin via non-canonical mechanisms) using ClustalW and Boxshade revealed a conserved putative SLIM [PGxF] (left), which was implicated in binding the PTB module of Tensin (NMR of DLC1-bound Tensin co-complex, right). (B) Bar diagram showing the various modules in GIV. The PGxF SLIM is located within the C-terminal stretch of GIV, which is largely disordered (see Figures S2A–S2C).

**Figure 2. *Continued***

(C) Sequence alignment of the C terminus of GIV shows that the PGxF SLIM is evolutionarily young (only conserved in higher organisms). The relative positions of this and other SLIMs (that bind G proteins, PI3-kinase) and modules (that facilitate RTK binding) within the intrinsically disordered C terminus are shown in Figure S2D.

(D) GST pull-down assays were performed using lysates of Cos7 cells as source of full-length GIV with GST-Tensin-3 SH2 and SH2+PTB fragments. Bound proteins were analyzed by immunoblotting with anti-His mAb.

(E) GST pull-down assays were performed using WT or $^{1741}$PGxA$^{1744}$ (F1744A) mutant His-GIV-CT and GST-Tensin-3 (SH2+PTB).

(F) GST pull-down assays were performed using WT or $^{1741}$PGxA$^{1744}$ (F1744A) mutant His-GIV-CT and GST-Kindlin-2 (F3-PTB).

(G) Bar graphs display the relative binding of His-GIV-CT to GST proteins in (F). Data are represented as mean ± SEM (n = 5); **p=<0.01.

(H) GST pull-down assays were performed using of His-GIV-CT WT or various mutants targeting its PGxF sequence and GST-Kindlin-2 (F3-PTB).

(I–K) GST pull-down assays were performed using GST-K2 (aa 571–680, [I]) and aa 564–680, [J]) WT or a QW/AA mutant proteins immobilized on glutathione beads and His-GIV-CT (aa 1,660–1,870). Bound proteins were analyzed as in (D). Bar graphs (K) display the relative binding of His-GIV-CT to GST-K2 proteins in (H) and (I). Data are represented as mean ± SEM (n = 5); **p=<0.01.

(L) A structural model built using the solved structures of DLC1-bound Tensin and Integrin-bound K2 as templates predicted that the FERM3-PTB module of K2 (gray ribbon) may simultaneously bind the non-canonical PGxF sequence within the C terminus of GIV (red) as well as the canonical NPxY sequence on the cytoplasmic tail of β1-integrins (black) via two distinct binding surfaces. These surfaces are exposed also when K2 is dimerized (see also Figure S4).

on the cell surface was diminished in MDA-MB-231 cells without GIV (Figures 1H–1J). When we monitored by immunofluorescence the recruitment of endogenous K2 in these cells, we unexpectedly found that the colocalization of active β1 and K2 was also reduced in GIV-depleted cells (Figure 1H), indicating that GIV may somehow enable the formation of active β1-integrin●K2 complexes at the FAs. Although the levels of total β1-integrin were reduced at the cell periphery in GIV-depleted cells, immunoblots revealed that the levels of the protein were not reduced (Figure 1F) but instead redistributed to vesicular structures at the center of the cell, which could represent some endocytic compartment. Although GIV-depleted cells did not always spread as well (quantified later in-depth), the findings in Figures 1G–1H were observed in GIV-depleted cells that had spread to an equivalent degree as control cells, indicating that GIV may impact integrin activation and K2 recruitment to integrins regardless of cell spreading. Taken together, we conclude that GIV is recruited to the cytoplasmic tails of β1-integrin indirectly via its ability to bind the K2 adaptor and that GIV may be a necessary component of integrin activation and for the formation of active-β1●K2 complexes. Furthermore, depletion of GIV was associated with reduced activation of β1-integrin in two additional cell lines, HeLa and Cos7, both previously used to study GIV's role in downstream integrin signaling (Lopez-Sanchez et al., 2015; Midde et al., 2018) (Figure S1C). These findings suggest that our findings in MDA-MB-231 cells may be relevant in other cell lines.

## The C Terminus of GIV Binds Kindlin's FERM3-PTB Domain via a Non-canonical Short Linear Motif

β1-Integrins bind the FERM3-PTB modules of talin and kindlin via canonical mechanisms that involve two conserved NPxY motifs on the cytoplasmic tail of the receptor. Because GIV lacks a similar motif, we hypothesized that the mechanism of GIV●K2 interaction may be non-canonical. The first clues into the mechanism came from a previously solved NMR structure of tensin-PTB bound to a peptide derived from the protein Deleted in Liver Cancer (DLC1) revealing a non-canonical mode of binding to PTB/FERM3-PTB modules (Chen et al., 2012). A sequence alignment showed that the core sequence "Pro(P)-Gly(G)-x-Phe(F)" in DLC1 that was previously implicated in binding tensin-PTB was evolutionarily conserved within the C terminus of GIV (Figures 2A–2C); the Phe(F) within this motif was determined to contribute significantly to the strength of the interaction by filling a shallow pocket within the PTB domain of tensin (Figure 2A). This putative PTB-binding short linear interaction motif (SLIM) in GIV-CT is situated downstream of the GEM motif that GIV uses to bind and activate Gαi and is within a stretch of sequence that was predicted to have the highest degree of disorder (Figures S2A–S2C). This region has previously been shown to also fold into an SH2-like module upon recognizing phosphotyrosines on the cytoplasmic tails of diverse ligand-activated growth factor RTKs (Lin et al., 2014) (Figure S2D). This motif also appeared to be evolutionarily young, i.e., conserved only in higher mammals (Figure 1C), much like GIV's SH2-like module (Lin et al., 2014).

We asked if the putative PTB-binding SLIM in GIV-CT is functional. First, using GST-tagged SH2 and PTB fragments of tensin, we confirmed that full-length GIV specifically binds the PTB domain of tensin (Figure 2D). We found that the wild-type (WT), but not a mutant, His-GIV-CT protein in which the Phe(F) within the PGxF sequence is mutated to alanine (PGxA) could bind GST-Tensin-PTB (Figure 2E), which confirmed that the tensin-PTB●GIV-CT interaction is direct that it requires the intact PGxF SLIM. When we carried out similar assays, but replaced GST-tensin-PTB with GST-K2-FERM3-PTB, we observed identical results

(Figures 2F and 2G), which confirmed that the K2-FERM3-PTB●GIV-CT interaction is also direct and that it too requires the intact PGxF SLIM. Using pull-down assays with GST-K2 and an array of His-tagged GIV-CT mutants that perturb the core PGxF SLIM, we further determined the relative contributions of the various residues within the SLIM: mutating the Pro(P) and Gly(G) to Ala(A) had a partial effect on the interaction, whereas mutating the Phe(F) was the most disruptive (Figure 2H). As expected, based on the location of the PGxF motif within the C terminus of GIV (Figure S2D), none of the mutants impacted GIV's ability to bind Gαi (Figure S3). These studies provided the rationale for the use of the PGxA single point mutant in all further studies as a precise tool to specifically dissect the functional relevance of the GIV●K2 interaction.

We then asked if perturbing the PTB-like conformation within the FERM3 module of K2 impacts the GIV●K2 interaction. To this end, we used a previously validated mutant in which $Glu(Q)^{614}Try(W)^{615}$ is mutated to AA in the FERM3 subdomain of K2, which impairs PTB-like folding and recognition of canonical NPxY sequences on β-integrins (Ma et al., 2008; Shi et al., 2007). Defective integrin activation in cells expressing this K2 mutant has previously been attributed to its inability to assemble the K2●β-integrin interface (Bledzka et al., 2016; Xu et al., 2014) (Ma et al., 2008; Shi et al., 2007; Montanez et al., 2008). Using two different GST-K2 constructs varying slightly in their construct boundaries (one K2 construct [aa 571–680; Figure 2I] was used by others to characterize the K2●β1 interaction *in vitro* and in cells [Montanez et al., 2008] and another construct was generated by us [aa 568–680; Figure 2J] and spans the complete FERM3 module), we found that this PTB-defective QW>AA mutant K2 is required for not just binding the NPxY sequence on β-integrins but also for binding GIV (Figures 2I–2K), indicating that the QW>AA K2 mutant is non-selective, in that the mutations impair both interactions indiscriminately. Because multiple groups observed impaired integrin activation in cells expressing the QW>AA K2 mutant, and we observe similar defects in activation in GIV-depleted cells (Figures 1G and 1H), it is possible that the observed defect in the QW>AA K2-expressing cells is not just due to impaired K2●β-integrin interaction but equally likely to be due to impaired K2●GIV interaction. Hence, to specifically study the impact of the GIV●K2 interaction, we used the newly identified PGxA point mutant of GIV that is deficient in binding to K2 in all subsequent assays.

## The GIV●Kindlin-2 Interaction Allosterically Enhances Kindlin's Affinity for β1-Integrin

Next, we asked if and how binding of GIV to K2 impacts the K2●β1-integrin interaction. Three possible scenarios were considered: (1) GIV and β1-integrin may compete for the same site or bind on overlapping sites on K2, and if so, their interactions will be mutually exclusive; (2) they may each bind K2 non-competitively via two interfaces without steric hindrances, and if so, they may bind concurrently and exist as ternary GIV●K2●β1-integrin complexes; (3) they may bind non-competitively at distinct sites on K2 but allosterically impact (either inhibit or augment) each other's' ability to bind K2. Superimposition of the DLC1(PGxF)●tensin complex structure (Chen et al., 2012), the recently solved β1●K2 co-complex structure (Li et al., 2017) and a homology model of K2 (built using tensin-PTB as a template [Figure 2L]), suggested that the canonical and non-canonical modes of binding of K2 to β1-integrin and GIV, respectively, may use two distinct interfaces and remain compatible with the assembly of ternary GIV●K2●β1-integrin complexes in both monomeric and dimeric states of K2 (Figure S4). We carried out a series of biochemical assays using recombinant proteins designed to look for intermolecular competition for interacting surfaces and/or the formation of co-complexes *in vitro*. In these assays, two components were kept constant, whereas the amount of the third component was varied. Increasing His-β1-CT (which contains the NPxY motif recognized by K2) did not displace His-GIV-CT from GST-K2; instead, we unexpectedly observed an enhanced coupling of GIV within a narrow range of concentration of β1-CT, exclusively when His-β1-CT and His-GIV-CT are both present in equimolar concentrations (Figure 3A). Similarly, increasing His-GIV-CT enhanced the coupling of His-K2 to GST-β1-CT only within a narrow range of concentration of His-GIV-CT, exclusively when His-K2 and His-GIV-CT are both present in equimolar concentrations (Figure 3B). Finally, when added in equimolar amounts, His-K2 enhanced the coupling of WT but not the PGxA mutant His-GIV-CT to GST-β1-CT (Figure 3C). Because these findings were observed consistently, with different protein preparations, the results appear to be most consistent with scenario #3; i.e., GIV and β1-CT may bind K2 non-competitively to assemble ternary complexes when present at optimal stoichiometry (Figures 3A–3C). Under the conditions tested, we found that binding of either protein to K2 allosterically augmented the binding of the other only when GIV, β1-CT, and K2 are all present in equimolar amounts (Figures 3A and 3B).

Next, we asked if the allosteric impact of the K2●GIV interaction we observe *in vitro* translates to augmentation of K2●β1-integrin interaction at FAs and β1 activation in cells. To this end, we monitored by

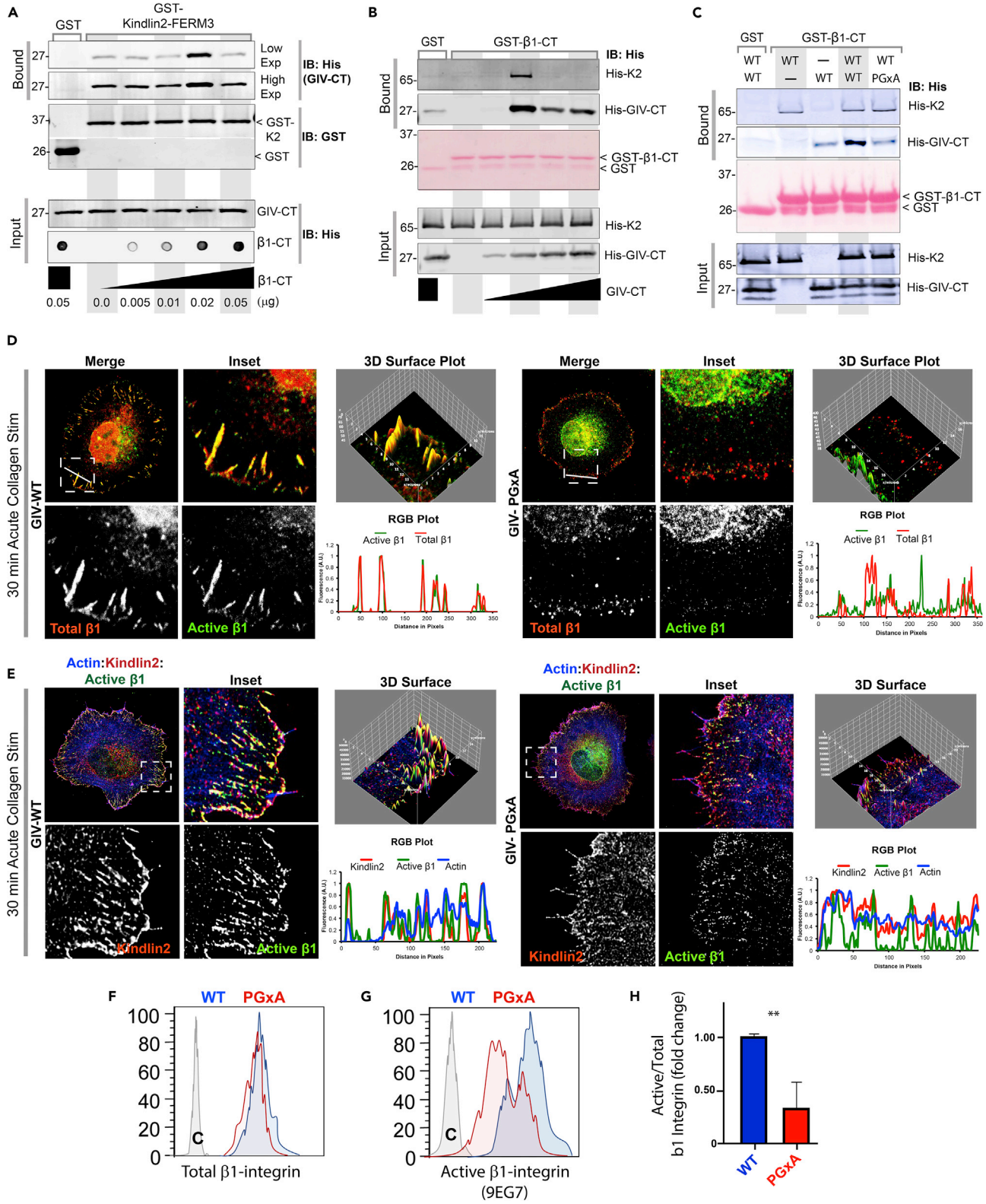
A
GST
GST-Kindlin2-FERM3
Bound
Input
Low Exp
High Exp
IB: His (GIV-CT)
< GST-K2
< GST
IB: GST
GIV-CT
β1-CT
IB: His
0.05
0.0
0.005
0.01
0.02
0.05 (μg)
B
GST
GST-β1-CT
IB: His
His-K2
His-GIV-CT
< GST-β1-CT
< GST
GIV-CT
C
GST
GST-β1-CT
WT
—
PGxA
D
Merge
Inset
3D Surface Plot
RGB Plot
Active β1
Total β1
30 min Acute Collagen Stim
GIV-WT
GIV- PGxA
Distance in Pixels
E
Actin:Kindlin2:
Active β1
3D Surface
Kindlin2
Actin
F
WT
PGxA
Total β1-integrin
G
Active β1-integrin
(9EG7)
H
Active/Total
b1 Integrin (fold change)
**

**Figure 3. The K2●GIV Interaction Allosterically Augments the K2●β1-integrin Interaction and *Vice Versa*, when Present in Equimolar Proportions, Enhances K2 Recruitment to Focal Adhesions and β1-Integrin Activation**

(A) GST pull-down assays were performed using fixed concentrations of GST-Kindlin-2-F3-PTB (GST-K2; 0.25 μg) and His-GIV-CT (aa 1,660–1,870; 1 μg) and increasing concentrations of His-β1-integrin tail, as indicated. Bound GIV was assessed by immunoblotting with anti-His mAb. Equal loading of His-GIV-CT was confirmed by SDS PAGE, and the increasing amounts of His-β1 was monitored by dot blot (input; lower panel).

(B) GST pull-down assays were performed using equal aliquots of GST-β1-integrin tail (2.5 μg) and full-length His-Kindlin 2 (K2) at equimolar concentrations and increasing amounts of His-GIV-CT (aa 1,660–1,870). GST-β1-bound proteins were assessed by immunoblotting using anti-His mAb and anti-GIV polyclonal Ab.

(C) GST pull-down assays were performed using GST-β1 in combination with His-GIV-CT-WT or PGxA (aa 1,660–1,870) and full-length His-Kindlin 2 (K2). GST-β1-bound proteins were assessed using anti-His mAb and anti-GIV polyclonal Ab.

(D and E) GIV-depleted MDA-MB-231 cells stably expressing Flag-GIV-WT or PGxA constructs were grown on poly-D-Lysine coated surface, resuspended and plated on collagen-coated coverslips for 30 min, fixed, and stained for active β1-integrin (green; using a conformational specific antibody, clone 9EG), phalloidin (blue; actin), and either total β1-integrin (D; red) or kindlin-2 (E; red) and analyzed by confocal microscopy. Representative deconvolved images are shown. Insets were analyzed by rendering 3D surface plots, and line scans were taken to generate RGB plots using ImageJ.

(F and G) FACS histograms of cells in (D) showing cell-surface expression of total (F) and active β1 (G), as measured by 9EG7 staining. C, IgG negative control.

(H) Bar graphs showing fold change in the proportion of activation of β1-integrin (active/total) in (F) and (G). Data are represented as mean ± SEM (n = 4); **p = < 0.01.

immunofluorescence activation of β1-integrins in response to collagen and the recruitment of endogenous K2 to these active receptors in GIV-depleted MDA MB-231 cells stably expressing GIV-WT or PGxA. We found that, compared with cells expressing GIV-WT, those expressing GIV-PGxA had reduced integrin clustering and activation, as determined using conformational anti-CD29 9EG7 antibodies (Figure 3D). As expected, with fewer active β1-integrins, the extent of β1●K2 co-localization was also reduced (Figure 3E). FACS analyses further confirmed that the extent of activation of β1-integrin was indeed suppressed in the GIV-PGxA mutant (Figures 3F–3H). Together, these findings indicate that the K2●GIV interaction augments the formation of GIV●K2●β1 complexes and is required for maximal activation of β1-integrins in cells. Such augmentation may be highly regulated by protein stoichiometry and only occur within narrow ranges of protein concentrations. These findings are in keeping with prior observations that much like K2 depletion, K2 overexpression can also cause suppression of β1-integrin activation (Harburger et al., 2009).

## The GIV●Kindlin-2 Interaction Enhances Tumor Cell Adhesion, Invasion, Integrin Signaling

Next, we asked how the newly defined GIV●kindlin-2 interaction impacts cellular phenotypes. Prior studies have shown that GIV is required for signal amplification downstream of ligand-activated β1-integrins via its ability to directly bind and activate Gαi and Class 1 PI3-kinase; the readouts used were cell adhesion and spreading; haptotaxis; activation of the PI3K→Akt, FAK→pY1764GIV, and RhoA→myosin light chain (MLC2) signaling axes; the degree of maturation of FAs with sequential recruitment of paxillin and vinculin proteins; and activation of FAK (Leyme et al., 2015, 2016; Lopez-Sanchez et al., 2015). If these downstream events were dependent on GIV's ability to bind ligand-activated β1-integrins, we hypothesized that uncoupling GIV from β1-integrins will impair them all. Alternatively, if GIV's ability to trigger G protein and PI3K signaling is independent of its ability to bind and activate β1-integrins, we expected that uncoupling GIV from β1-integrins will have little or no impact on these readouts. To determine which scenario may be true, we analyzed these readouts in GIV-depleted MDA MB-231 cells (by a shRNA targeting its 3′ UTR [Figure 4A]; Lopez-Sanchez et al., 2015) stably expressing GIV-WT and GIV-PGxA that were acutely stimulated by plating on collagen. We found that, much like shGIV cells, those expressing the GIV-PGxA mutant was impaired in cell adhesion (Figures 4A–4C), cell spreading (Figure 4D), and haptotaxis along a serum gradient through Matrigel inserts (Figures 4F–4I). These phenotypic changes were accompanied also by significant impairment of GIV (Figures 4J, 4K, S5A, and S5B) and Akt phosphorylation (Figures 4J and S5B), activation of FAK (Figures 4L and S5C), and phosphorylation of MLC2 (Figures 4M and S5D). We used phospho-MLC2 as a surrogate marker of RhoA activity because multiple prior studies (Ren et al., 1999; Danen et al., 2002; Bhadriraju et al., 2007) have shown that RhoA activity drops down to levels below detection during cell adhesion, and hence, monitoring pMLC2 is a more reliable readout of GIV-dependent RhoA activity during integrin signaling (Leyme et al., 2015). Because all these impairments we observed in cells expressing the K2-binding-deficient PGxA mutant of GIV were previously observed in cells without GIV, or those expressing single point mutants of GIV that selectively impair its ability to bind and activate Gαi and PI3K (see Figure 4M), we conclude that the GIV●K2 interaction may be an essential upstream event for integrin-coupled downstream activation of Gαi and PI3K. When the interaction is severed (as occurs in cells expressing the PGxA mutant GIV), none of the signaling pathways are effectively triggered, indicating that binding of GIV to integrins within the GIV●K2●β1 complexes is a pre-requisite step.

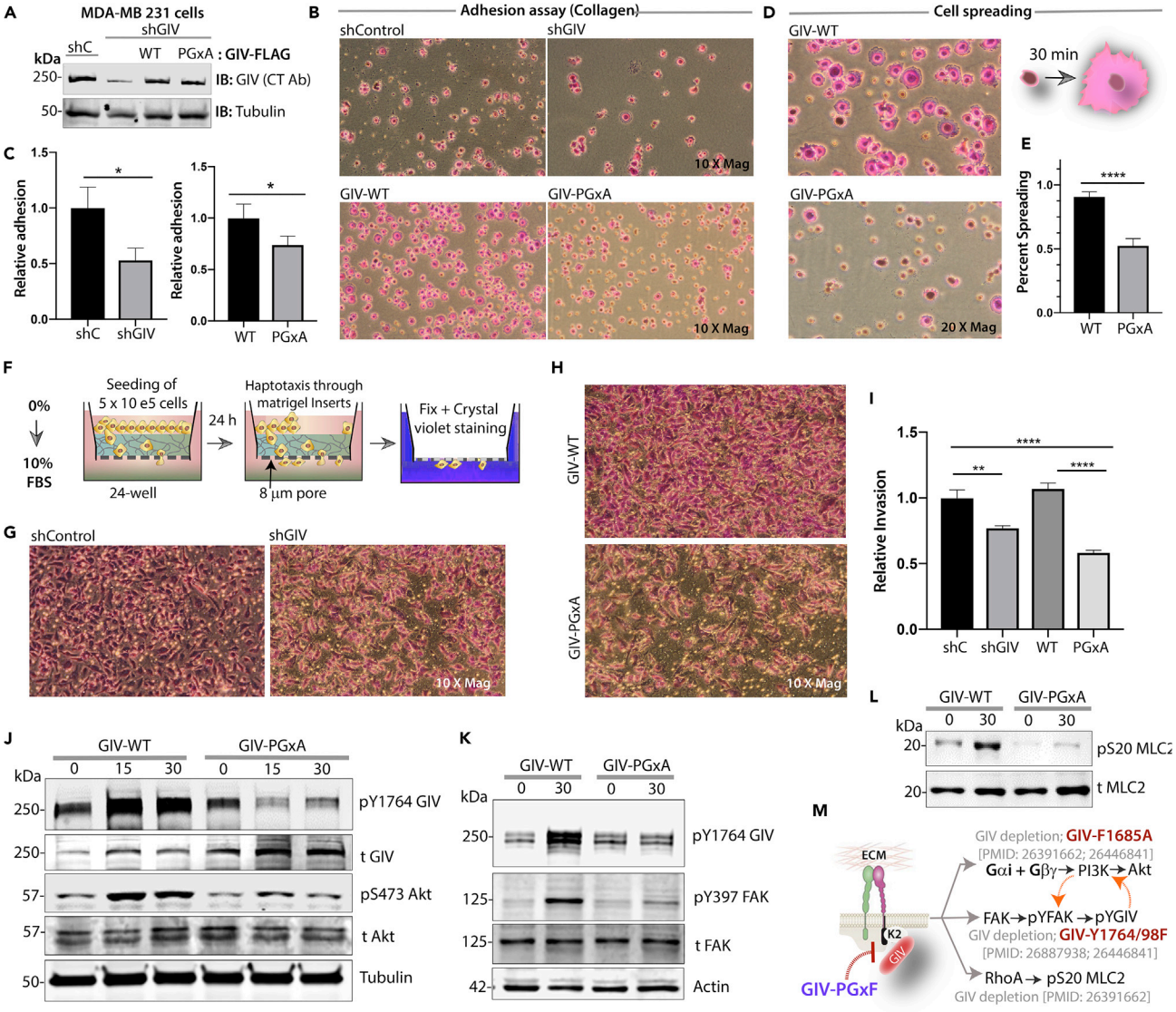


**Figure 4. The K2●GIV Interaction Is Required for Tumor Cell Adhesion, Spreading, and Invasion through the ECM**

(A) Whole-cell lysates of control (shC) or GIV-depleted (shGIV) MDA-MB 231 cells stably expressing GIV-WT or the K2-binding deficient PGxA mutant was analyzed for GIV and tubulin by immunoblotting.

(B) MDA-MB 231 cell lines in (A) were grown on poly-D-Lysine-coated surface, resuspended, and plated on 12-well collagen-coated plates for 30 min before being fixed in 4% PFA and stained with crystal violet. Cells were visualized and imaged by light microscopy. Representative images are shown.

(C) Bar graphs display the relative numbers of adherent cells per field, as determined using ImageJ. Data are represented as mean ± SEM (n = 4); *p = < 0.05

(D and E) Adherent MDA-MB 231 cells in (B) were further analyzed for attachment-induced cell spreading at higher magnification. Representative images are shown (D) and quantification of percent spreading is displayed as bar graph I. Data are represented as mean ± SEM (n = 4); ****p=<0.0001.

(F) Schematic diagram showing the serum gradient-induced haptotaxis assay conditions used in (G)–(I).

(G–I) MDA-MB 231 cell lines in (A) were analyzed for the ability to invade through Atrigel-coated transwells. The number of cells that successfully invaded within 24 h was imaged (G and H) and quantified using ImageJ and displayed as bar graphs (I). Data are represented as mean ± SEM (n = 4); **p=<0.01, ****p=<0.0001.

(J–L) MDA-MB 231 cells were grown on poly-D-Lysine and stimulated acutely by plating on collagen-coated plates as in (B) and lysed on plate after indicated periods of time, and equal aliquots of lysates were then analyzed for phospho(p) and total (t) proteins as indicated. See also Figure S5 for quantification of biologically independent experiments.

(M) Schematic summarizing the post-receptor pathways previously shown to be impacted by GIV, and the specific approaches (GIV depletion or mutants) that were used to conclude the same. Orange arrows: Positive feedforward loop of signaling. The mutation F1685A specifically impairs GIV's ability to bind and activate Gαi (Garcia-Marcos et al., 2009). The mutation Y1764/98F specifically impairs GIV's ability to bind and activate PI3K (Lin et al., 2011) and enhance the PI3K↔FAK feedforward loop (Lopez-Sanchez et al., 2015).

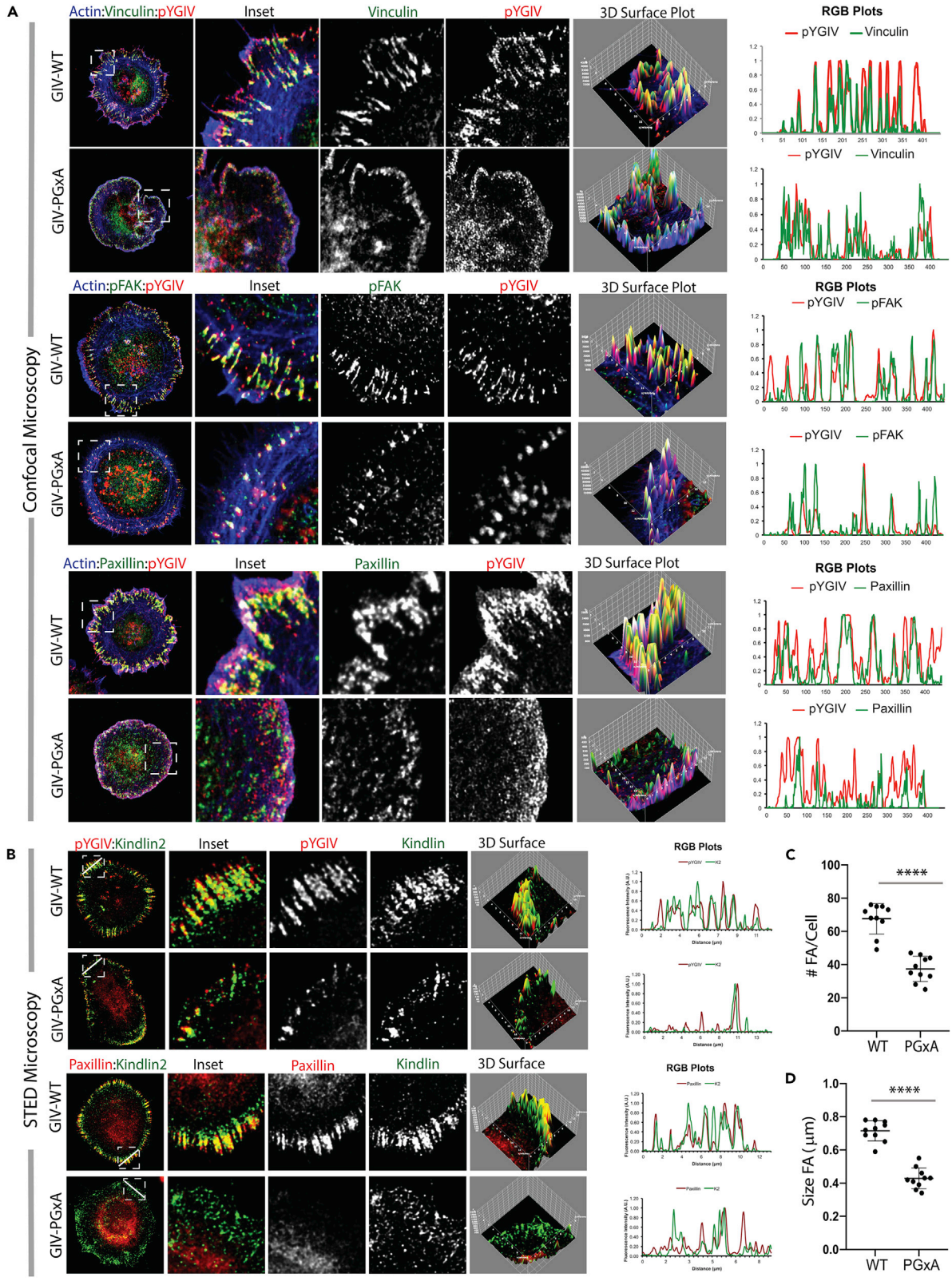
A
Confocal Microscopy
Actin:Vinculin:pYGIV
Inset
Vinculin
pYGIV
3D Surface Plot
RGB Plots
pYGIV
Vinculin
GIV-WT
GIV-PGxA
Actin:pFAK:pYGIV
Inset
pFAK
pYGIV
3D Surface Plot
RGB Plots
pYGIV
pFAK
GIV-WT
GIV-PGxA
Actin:Paxillin:pYGIV
Inset
Paxillin
pYGIV
3D Surface Plot
RGB Plots
pYGIV
Paxillin
GIV-WT
GIV-PGxA
B
STED Microscopy
pYGIV:Kindlin2
Inset
pYGIV
Kindlin
3D Surface
RGB Plots
GIV-WT
GIV-PGxA
Paxillin:Kindlin2
Inset
Paxillin
Kindlin
3D Surface
RGB Plots
GIV-WT
GIV-PGxA
C
# FA/Cell
****
WT
PGxA
D
Size FA (µm)
****
WT
PGxA

**Figure 5. The K2●GIV Interaction Is Necessary for the Maturation of Focal Adhesions (FA) and for Triggering the FA-Localized FAK→pYGIV Signals**

(A) GIV-depleted MDA-MB-231 cells stably expressing GIV-WT or GIV-PGxA constructs were grown on poly-D-Lysine-coated surface, resuspended, and plated on collagen-coated coverslips for 30 min, fixed, and stained for phalloidin (actin; blue), bona fide FA structural or signaling components (i.e., Vinculin [top], pYFAK [Y397; middle], or Paxillin [lower]; green), and pYGIV (red) and analyzed by confocal microscopy. Representative deconvolved images are shown. Insets were analyzed by rendering 3D surface plots, and line scans were taken to generate RGB plots, both using ImageJ.

(B) STED super-resolution microscopy was carried out on cells in (A) to analyze K2 colocalization with pYGIV (top) or paxillin (bottom). Representative deconvolved images are shown. Insets were analyzed by rendering 3D surface plots and RGB plots as in (A).

(C and D) The Paxillin-stained images in (A) were used to quantify focal adhesion plaque number (C) and size (area; D) with ImageJ.

Consistent with the observed impairment in integrin signaling, we also found by immunofluorescence/confocal microscopy that the abundance of paxillin and vinculin-positive structures and the activation of FAK in the PGxA-cells were reduced (Figure 5A). To determine if the GIV●K2 interaction persists later in mature FAs, we used two-color super-resolution stimulated emission depletion (STED) microscopy (Hell and Wichmann, 1994; Klar et al., 2000) enabling a lateral resolution of ~40 nm to assess nanoscale co-localization of endogenous pYGIV and K2 within focal adhesions. Prior studies using STED (Spiess et al., 2018; Colin-York et al., 2017) have revealed the superiority of this approach over conventional microscopy for assessing the organization of FAs into nanometer-sized clusters of multi-protein assemblies. We observed nanoscale co-localization between pYGIV and K2 within mature FA-structures that were positive for paxillin (Figure 5B); compared with GIV-WT cells, such structures were far fewer and virtually lacking in cells expressing the PGxA mutant. Quantification of these paxillin-positive structures confirmed a significant reduction in the number and size of mature FA-like structures in the PGxA cells (Figures 5C and 5D).

Taken together, these findings implicate the GIV●K2 interaction in some of the earliest "upstream" events that begin within nascent FAs, i.e., enhanced recruitment of K2 to active β1, formation of GIV●K2●β1-integrin complexes, and integrin clustering and activation. Consequently, a myriad of "downstream" events within mature FAs are also derailed, e.g., their number and size; phosphoactivation of MLC, Akt, and FAK; and the activation of a previously defined feedforward loop (FAK↔pYGIV↔PI3K↔FAK [Leyme et al., 2016; Lopez-Sanchez et al., 2015]). It is certainly possible that some of the post-receptor activation pathway/downstream signaling in PGxA mutant cells may reflect some of the impact of GIV's ability to bind the PTB domain of Tensin. However, the observed impact of GIV-PGxA on integrin activation observed earlier (Figures 3D and 3E) is unlikely to be due to GIV●Tensin interaction because tensin is recruited much later (Torgler et al., 2004) than the time points studied here and in mature focal adhesions (unlike GIV, which colocalizes with β1-integrin in nascent adhesions at the cell periphery [Lopez-Sanchez et al., 2015]) has been shown to be a part of downstream signaling pathway (Bockholt and Burridge, 1993) and is considered as largely dispensable for the early steps of integrin activation (Theodosiou et al., 2016; Calderwood et al., 2013).

## The GIV●Kindlin-2●β1-Integrin Synergy May Have a Poor Prognosis in Breast Cancer

Next, we asked if the observed allosteric synergy between GIV, K2, and β1-integrin we observe here and the impact of such synergy on sinister properties of tumor cells can be meaningful when assessing tumor behavior and/or prognosticating clinical outcome. First, we asked if the levels of expression of each of these three entities alone, or in combination, could impact one of the most important readouts of cancer aggressiveness, i.e., metastasis-free patient survival. To discern this, we chose to study a pooled cohort of patients (Minn et al., 2005; Bos et al., 2009; Wang et al., 2005) with breast cancers who did not receive adjuvant chemotherapy, and hence, in them metastatic progression reflects natural disease progression and not resistance/selection under treatment. Samples were divided into "low" and "high" subgroups with regard to GIV (CCDC88A; Figure 6A), β1-integrin (ITGB1; Figure 6B) and K2 (FERMT2; Figure 6C) gene expression levels using the StepMiner algorithm (Sahoo et al., 2007), implemented within the hierarchical exploration of gene-expression microarrays online (HEGEMON) software (Dalerba et al., 2011; Volkmer et al., 2012). Kaplan-Meier analyses of the disease-free survival showed that high levels of expression of each alone was enough to carry a grave prognosis, i.e., a shorter metastasis-free survival (Figures 6A–6C). To determine if the levels of expression of these genes and a few other important genes implicated in some of the earliest steps of integrin activation interact synergistically as independent variables to impact survival of patients, we carried out a Cox proportional-hazards model (Cox, 1972), which is a regression model that is commonly used as a statistical method for investigating the effect of several variables upon the time it takes for a specified event to happen, in this case, metastasis (Cox, 1972). We found that, in this model, CCDC88A (GIV) significantly interacts with FERMT2 (K2), ITGB1 (β1-integrin), and

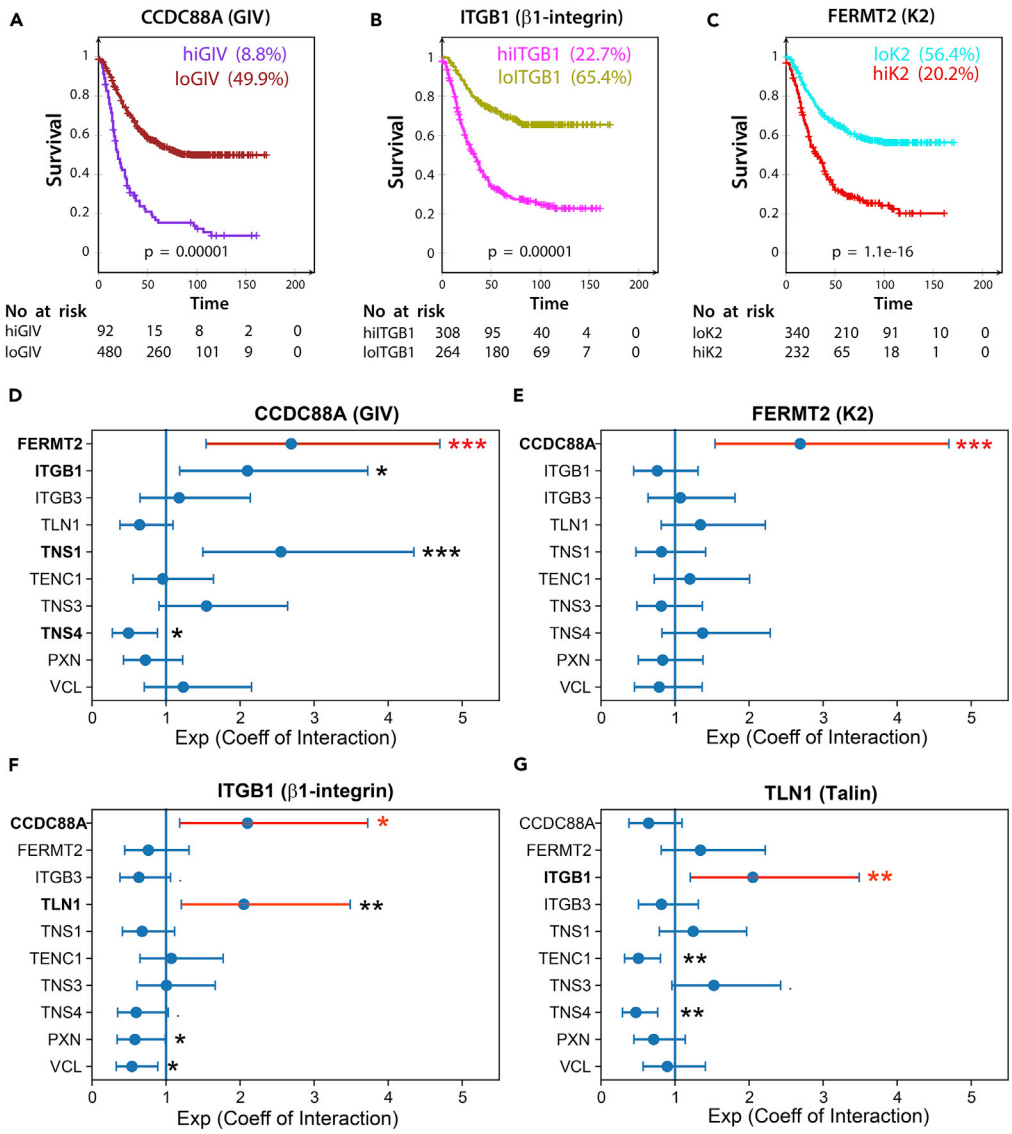


**Figure 6. Levels of Expression of GIV, Kindlin-2, and β1-integrin Prognosticate Progression to Metastasis**

Primary breast cancers from 572 patients (three independent cohorts, pooled [Minn et al., 2005; Bos et al., 2009; Wang et al., 2005]) who did not receive adjuvant therapy were segregated into groups of high versus low expression (see Methods) of target genes and analyzed for metastasis-free survival.

(A–C) Kaplan-Meier curves for metastasis-free survival over time among patients whose primary tumors had high versus low levels of GIV (CCDC88A; A), β1-integrin (ITGB1; B) and K2 (FERMT2; C).

(D–G) Statistical interaction (synergy between variables) is measured in the Cox proportional hazards regression model for CCDC88A (GIV; D), FERMT2 (K2; E), ITGB1 (β1-integrin; F), and TLN1 (talin; G) with other major genes involved in some of the earliest steps of integrin activation and the formation and maturation of the FAs. Coefficient of the interaction term in Cox regression models is plotted with 95% confidence interval that demonstrates the significance of the statistical interaction. ***p = 0.001; **p = 0.01; *p = 0.05.

TNS1, 4 (tensin) but not TLN1 (talin) (Figure 6D); FERMT2 (K2) only interacts with GIV (Figure 6E). ITGB1 interacted with GIV and tensin (Figure 6F); talin interacted primarily with ITGB1 (Figure 6G). Thus, of all the gene pairs tested, high GIV and K2 expression had a synergistic impact on shortening metastasis-free survival. These findings not only provide evidence for "interaction" between GIV and K2 at the levels of gene expression and expose its impact on survival outcome but also serves to further cement the role of the GIV●K2 interaction in tumor aggressiveness and progression to metastasis. Findings are also consistent with prior evidence that elevated levels of K2 carries a poor prognosis in a variety of cancers (Yan et al.,

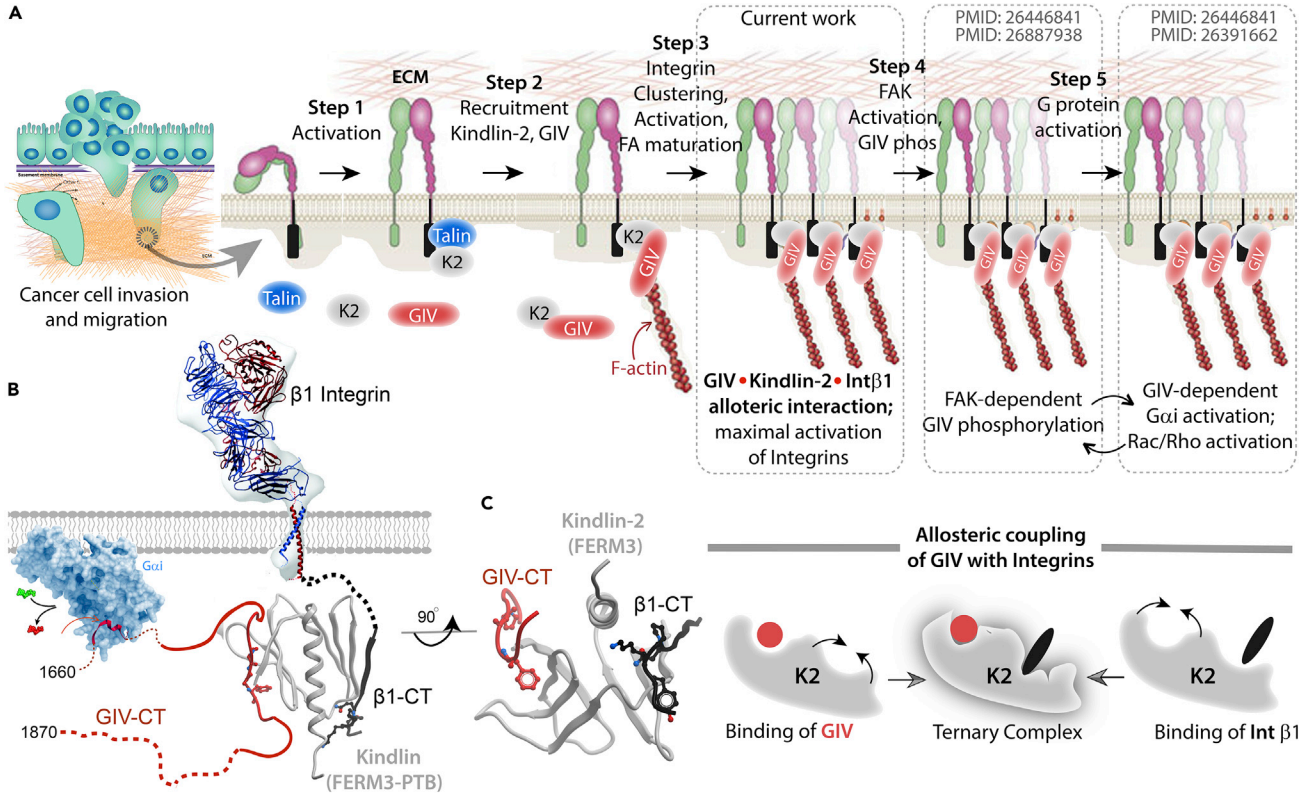


**Figure 7. Schematic Summarizing How GIV Impacts Early and Late Events in β1-integrin Signaling**

(A) Schematic illustrating the role of GIV during various steps of β1-integrin activation and signaling. Integrin activation is mediated by binding of its cytoplasmic tail to Talin (Step 1) and GIV●K2 complexes (Step 2). The latter is necessary for integrin clustering, activation, and maturation of focal adhesions (Step 3); activation of FAK; and tyrosine phosphorylation of GIV (Step 4). Previously described forward feedback loops (Step 5) orchestrated by G protein signaling further enhances integrin signaling.

(B) Structural basis for how ligand-activated β1-integrins may bind and modulate trimeric G protein, Gαi via the assembly of K2●GIV complexes.

(C) Binding of either GIV or β1-integrin on non-overlapping interfaces of K2 allosterically enhances the formation of GIV●K2●β1-integrin complexes.

2016; Zhan et al., 2015; Ge et al., 2015; Cao et al., 2015; Ma et al., 2015b; Mahawithitwong et al., 2013; Shen et al., 2012; Sin et al., 2011; Talaat et al., 2011).

## Conclusions

The major discovery we report herein is the mechanism and consequences of a direct interaction between GIV and K2. Using selective single point mutants of GIV that are incapable of binding K2, we chart the two major consequences of this GIV●K2 interaction. First, the GIV●K2 interaction impacts GIV biology because it appears to be a pre-requisite for the previously defined GIV-dependent signaling programs downstream of ligand-activated integrins, e.g., G protein (Gβγ→PI3K), PI3K→Akt, PI3K→FAK→pYGIV, and RhoA→MLC. Second, this interaction impacts integrin biology because it augments the affinity of K2 for the cytoplasmic tail of β1-integrins *in vitro*, the recruitment of K2 to β1-integrins in cells, and its subsequent clustering and activation within nascent and mature FAs.

As for the impact of the GIV●K2 interaction on GIV biology, findings showcased here, together with our understanding of how GIV modulates integrin/FAK signaling via G protein intermediates (Leyme et al., 2015, 2016; Lopez-Sanchez et al., 2015), provide a more complete mechanistic insight into the roles of GIV in both early and late steps of integrin signaling (Figure 7A). Because integrin signaling aids cancer growth, metastasis, and drug resistance, the signaling interfaces assembled by GIV (GIV●K2 and GIV●■ Gαi) provide potentially impactful strategies for targeting the integrin pathway. Furthermore, GIV's FERM3/PTB-binding PGxF motif provides the second mechanism (GIV's SH2-like module was the first [Lin et al., 2014]) by which GIV can couple Gα-proteins to non-GPCRs like integrins (Figure 7B), which are typically believed to initiate tyrosine-based signals. Because GIV binds the PTB domain of tensin, it is

possible that the SLIM in GIV we define here, which binds K2-FERM3-PTB and tensin-PTB, may also recognize other PTB-module-containing adaptors. If so, it is possible that such versatility of the motif could enable coupling of GIV/G proteins, PI3K activation, and RhoA-dependent actin remodeling to diverse classes of non-GPCRs besides integrins that also use PTB proteins as adaptors, i.e., cytokine, LDL-receptor, leukocyte receptors, and RTKs (Smith et al., 2006), leading to signal convergence.

As for the impact of the GIV●K2 interaction on integrin biology, its ability to allosterically augment the affinity of K2 for β1-integrins and enhance the activation of β1-integrins resembles how talin-dependent activation of β1-integrins is triggered by adjusting the affinity of talin for integrins. For example, binding of talin's FERM domain to charged acidic phospholipids, phosphatidylinositol 4,5-bisphosphate(PtdIns(4,5)P2), greatly increased its affinity for integrins, so that once talin is recruited to the plasma membrane, this phospholipid could augment the formation of talin-integrin complexes (Moore et al., 2012; Ye et al., 2016). In fact, membrane recruitment of talin is sufficient to increase its affinity for integrins (Lagarrigue et al., 2016; Lee et al., 2009; Han et al., 2006).

In the case of K2, researchers generally agree that K2's adaptor functions may be critical for maximal integrin activation and clustering (reviewed in Calderwood et al. [2013]), but how the K2●β1-integrin interaction augments integrin activation remained unknown (Bledzka et al., 2012; Kahner et al., 2012). We have not only pinpointed GIV as one binding partner that adjusts the affinity of K2 for β1-integrins but also provided a molecular basis for how such adjustment of affinity is brought about through an intramolecular allostery within K2 (Figure 7C). Our findings that GIV and β1-integrin may augment each other's ability to bind K2-FERM3-PTB suggest that the interplay between integrin, K2, and GIV may serve as one of the long-sought missing early steps in integrin activation.

### Limitations of the Study

Despite gaining meaningful structural insights into the nature of the GIV●K2 interface, we were unable to generate a Kindlin construct that would selectively disrupt its ability to bind GIV without interrupting its ability to bind β1 integrins. Because our experiments showed that the GIV●K2 and K2●β1 interfaces allosterically modulate each other, generation of such specific K2 mutants may not be possible altogether. Whether GIV modulates other receptors that also use FERM3-PTB domain containing adaptors to relay downstream signals was not investigated in this study; it is possible that some of the phenotypes in cells expressing GIV mutants that cannot bind FERM3-PTB domains is due to convergent signaling downstream of other receptors that use such adaptors. Finally, it is possible that GIV also binds other PTB-domain containing adaptors. Whether this is possible is an ongoing investigation.

### Resources Availability

#### *Lead Contact*

Pradipta Ghosh, M.D. prghosh@ucsd.edu.

#### *Materials Availability*

Any materials generated and used in this study are available for dissemination to others.

#### *Data and Code Availability*

Not applicable.

## METHODS

All methods can be found in the accompanying Transparent Methods supplemental file.

## SUPPLEMENTAL INFORMATION

Supplemental Information can be found online at https://doi.org/10.1016/j.isci.2020.101209.

## ACKNOWLEDGMENTS

This paper was supported by NIH CA238042, AI141630, CA100768, and CA160911 (to P.G). C.R. was supported by an NCI/NIH-funded Cancer Therapeutics Training ($CT^2$) Training Program (T32 CA121938) and an NIDDK/NIH-funded training grant (T32 DK007202). N.K. was supported by an NIH predoctoral

fellowship (F31 CA206426) and T32 training grants T32CA067754 and T32DK007202. S.R. was supported by NIH awards R01– AI118985 and GM117424 (to Handel and Kufareva) and in part by an intramural UC San Diego Chancellor's Center Launch Funds. We thank Ying Dunkel and Nina Sun for technical support in this work. We also thank Dr. Irina Kufareva at Skaggs School of Pharmacy and Pharmaceutical Sciences for insightful discussions during the work.

## AUTHOR CONTRIBUTIONS

C.R., N.K., N.R., and P.G. designed, executed, and analyzed most of the experiments in this work. S.R. cloned and purified His-Kindlin and GST-kindlin constructs, and both I.L.-S. and S.R. performed pull-down studies with WT and mutant Kindlin constructs. C.R., N.K., and P.G. conceived the project. C.R. and S.R. wrote materials and methods and edited the manuscript. P.G. wrote the manuscript.

## DECLARATION OF INTERESTS

The authors declare no competing interests.

Received: March 15, 2020
Revised: April 15, 2020
Accepted: May 24, 2020
Published: June 26, 2020

## REFERENCES

Bachir, A.I., Zareno, J., Moissoglu, K., Plow, E.F., Gratton, E., and Horwitz, A.R. (2014). Integrin-associated complexes form hierarchically with variable stoichiometry in nascent adhesions. Curr. Biol. *24*, 1845–1853.

Bhadriraju, K., Yang, M., Alom Ruiz, S., Pirone, D., Tan, J., and Chen, C.S. (2007). Activation of ROCK by RhoA is regulated by cell adhesion, shape, and cytoskeletal tension. Exp. Cell Res. *313*, 3616–3623.

Bledzka, K., Bialkowska, K., Sossey-Alaoui, K., Vaynberg, J., Pluskota, E., Qin, J., and Plow, E.F. (2016). Kindlin-2 directly binds actin and regulates integrin outside-in signaling. J. Cell Biol. *213*, 97–108.

Bledzka, K., Liu, J., Xu, Z., Perera, H.D., Yadav, S.P., Bialkowska, K., Qin, J., Ma, Y.Q., and Plow, E.F. (2012). Spatial coordination of kindlin-2 with talin head domain in interaction with integrin beta cytoplasmic tails. J. Biol. Chem. *287*, 24585–24594.

Bockholt, S.M., and Burridge, K. (1993). Cell spreading on extracellular matrix proteins induces tyrosine phosphorylation of tensin. J. Biol. Chem. *268*, 14565–14567.

Bos, P.D., Zhang, X.H., Nadal, C., Shu, W., Gomis, R.R., Nguyen, D.X., Minn, A.J., Van de Vijver, M.J., Gerald, W.L., Foekens, J.A., and Massague, J. (2009). Genes that mediate breast cancer metastasis to the brain. Nature *459*, 1005–1009.

Bottcher, R.T., Veelders, M., Rombaut, P., Faix, J., Theodosiou, M., Stradal, T.E., Rottner, K., Zent, R., Herzog, F., and Fassler, R. (2017). Kindlin-2 recruits paxillin and Arp2/3 to promote membrane protrusions during initial cell spreading. J. Cell Biol. *216*, 3785–3798.

Calderwood, D.A., Campbell, I.D., and Critchley, D.R. (2013). Talins and kindlins: partners in integrin-mediated adhesion. Nat. Rev. Mol. Cell Biol. *14*, 503–517.

Campbell, I.D., and Humphries, M.J. (2011). Integrin structure, activation, and interactions. Cold Spring Harb. Perspect. Biol. *3*, a004994.

Cao, H.H., Zhang, S.Y., Shen, J.H., Wu, Z.Y., Wu, J.Y., Wang, S.H., Li, E.M., and Xu, L.Y. (2015). A three-protein signature and clinical outcome in esophageal squamous cell carcinoma. Oncotarget *6*, 5435–5448.

Chen, L., Liu, C., Ko, F.C., Xu, N., Ng, I.O., Yam, J.W., and Zhu, G. (2012). Solution structure of the phosphotyrosine binding (PTB) domain of human tensin2 protein in complex with deleted in liver cancer 1 (DLC1) peptide reveals a novel peptide binding mode. J. Biol. Chem. *287*, 26104–26114.

Colin-York, H., Eggeling, C., and Fritzsche, M. (2017). Dissection of mechanical force in living cells by super-resolved traction force microscopy. Nat. Protoc. *12*, 783–796.

Cox, D.R. (1972). Regression models and life tables (with discussion). J. R. Statist Soc. B *34*, 187–220.

Dalerba, P., Kalisky, T., Sahoo, D., Rajendran, P.S., Rothenberg, M.E., Leyrat, A.A., Sim, S., Okamoto, J., Johnston, D.M., Qian, D., et al. (2011). Single-cell dissection of transcriptional heterogeneity in human colon tumors. Nat. Biotechnol. *29*, 1120–1127.

Danen, E.H., Sonneveld, P., Brakebusch, C., Fassler, R., and Sonnenberg, A. (2002). The fibronectin-binding integrins alpha5beta1 and alphavbeta3 differentially modulate RhoA-GTP loading, organization of cell matrix adhesions, and fibronectin fibrillogenesis. J. Cell Biol. *159*, 1071–1086.

Enomoto, A., Murakami, H., Asai, N., Morone, N., Watanabe, T., Kawai, K., Murakumo, Y., Usukura, J., Kaibuchi, K., and Takahashi, M. (2005). Akt/PKB regulates actin organization and cell motility via Girdin/APE. Dev. Cell *9*, 389–402.

Fukuda, K., Bledzka, K., Yang, J., Perera, H.D., Plow, E.F., and Qin, J. (2014). Molecular basis of kindlin-2 binding to integrin-linked kinase pseudokinase for regulating cell adhesion. J. Biol. Chem. *289*, 28363–28375.

Garcia-Alvarez, B., de Pereda, J.M., Calderwood, D.A., Ulmer, T.S., Critchley, D., Campbell, I.D., Ginsberg, M.H., and Liddington, R.C. (2003). Structural determinants of integrin recognition by talin. Mol. Cell *11*, 49–58.

Garcia-Marcos, M., Ghosh, P., and Farquhar, M.G. (2009). GIV is a nonreceptor GEF for G alpha i with a unique motif that regulates Akt signaling. Proc. Natl. Acad. Sci. U S A *106*, 3178–3183.

Ge, Y.S., Liu, D., Jia, W.D., Li, J.S., Ma, J.L., Yu, J.H., and Xu, G.L. (2015). Kindlin-2: a novel prognostic biomarker for patients with hepatocellular carcinoma. Pathol. Res. Pract. *211*, 198–202.

Goksoy, E., Ma, Y.Q., Wang, X., Kong, X., Perera, D., Plow, E.F., and Qin, J. (2008). Structural basis for the autoinhibition of talin in regulating integrin activation. Mol. Cell *31*, 124–133.

Han, J., Lim, C.J., Watanabe, N., Soriani, A., Ratnikov, B., Calderwood, D.A., Puzon-McLaughlin, W., Lafuente, E.M., Boussiotis, V.A., Shattil, S.J., and Ginsberg, M.H. (2006). Reconstructing and deconstructing agonist-induced activation of integrin alphaIIbbeta3. Curr. Biol. *16*, 1796–1806.

Harburger, D.S., Bouaouina, M., and Calderwood, D.A. (2009). Kindlin-1 and -2 directly bind the C-terminal region of beta integrin cytoplasmic tails and exert integrin-specific activation effects. J. Biol. Chem. *284*, 11485–11497.

Hell, S.W., and Wichmann, J. (1994). Breaking the diffraction resolution limit by stimulated emission: stimulated-emission-depletion fluorescence microscopy. Opt. Lett. *19*, 780–782.

Kahner, B.N., Kato, H., Banno, A., Ginsberg, M.H., Shattil, S.J., and Ye, F. (2012). Kindlins, integrin activation and the regulation of talin recruitment to alphaIIbbeta3. PLoS One *7*, e34056.

Kalogriopoulos, N.A., Rees, S.D., Ngo, T., Kopcho, N.J., Ilatovskiy, A.V., Sun, N., Komives, E.A., Chang, G., Ghosh, P., and Kufareva, I. (2019). Structural basis for GPCR-independent activation of heterotrimeric Gi proteins. Proc. Natl. Acad. Sci. U S A *116*, 16394–16403.

Klar, T.A., Jakobs, S., Dyba, M., Egner, A., and Hell, S.W. (2000). Fluorescence microscopy with diffraction resolution barrier broken by stimulated emission. Proc. Natl. Acad. Sci. U S A *97*, 8206–8210.

Lagarrigue, F., Kim, C., and Ginsberg, M.H. (2016). The Rap1-RIAM-talin axis of integrin activation and blood cell function. Blood *128*, 479–487.

Lau, T.L., Dua, V., and Ulmer, T.S. (2008a). Structure of the integrin alphaIIb transmembrane segment. J. Biol. Chem. *283*, 16162–16168.

Lau, T.L., Partridge, A.W., Ginsberg, M.H., and Ulmer, T.S. (2008b). Structure of the integrin beta3 transmembrane segment in phospholipid bicelles and detergent micelles. Biochemistry *47*, 4008–4016.

Lee, H.S., Lim, C.J., Puzon-McLaughlin, W., Shattil, S.J., and Ginsberg, M.H. (2009). RIAM activates integrins by linking talin to ras GTPase membrane-targeting sequences. J. Biol. Chem. *284*, 5119–5127.

Legate, K.R., and Fassler, R. (2009). Mechanisms that regulate adaptor binding to beta-integrin cytoplasmic tails. J. Cell Sci. *122*, 187–198.

Leyme, A., Marivin, A., and Garcia-Marcos, M. (2016). GIV/Girdin (Galpha-interacting, vesicle-associated protein/girdin) creates a positive feedback loop that potentiates outside-in integrin signaling in cancer cells. J. Biol. Chem. *291*, 8269–8282.

Leyme, A., Marivin, A., Perez-Gutierrez, L., Nguyen, L.T., and Garcia-Marcos, M. (2015). Integrins activate trimeric G proteins via the nonreceptor protein GIV/Girdin. J. Cell Biol. *210*, 1165–1184.

Li, H., Deng, Y., Sun, K., Yang, H., Liu, J., Wang, M., Zhang, Z., Lin, J., Wu, C., Wei, Z., and Yu, C. (2017). Structural basis of kindlin-mediated integrin recognition and activation. Proc. Natl. Acad. Sci. U S A *114*, 9349–9354.

Lin, C., Ear, J., Midde, K., Lopez-Sanchez, I., Aznar, N., Garcia-Marcos, M., Kufareva, I., Abagyan, R., and Ghosh, P. (2014). Structural basis for activation of trimeric Gi proteins by multiple growth factor receptors via GIV/Girdin. Mol. Biol. Cell *25*, 3654–3671.

Lin, C., Ear, J., Pavlova, Y., Mittal, Y., Kufareva, I., Ghassemian, M., Abagyan, R., Garcia-Marcos, M., and Ghosh, P. (2011). Tyrosine phosphorylation of the Galpha-interacting protein GIV promotes activation of phosphoinositide 3-kinase during cell migration. Sci. Signal. *4*, ra64.

Lopez-Sanchez, I., Kalogriopoulos, N., Lo, I.C., Kabir, F., Midde, K.K., Wang, H., and Ghosh, P. (2015). Focal adhesions are foci for tyrosine-based signal transduction via GIV/Girdin and G proteins. Mol. Biol. Cell *26*, 4313–4324.

Ma, G.S., Aznar, N., Kalogriopoulos, N., Midde, K.K., Lopez-Sanchez, I., Sato, E., Dunkel, Y., Gallo, R.L., and Ghosh, P. (2015a). Therapeutic effects of cell-permeant peptides that activate G proteins downstream of growth factors. Proc. Natl. Acad. Sci. U S A *112*, E2602–E2610.

Ma, H.X., Shu, Q.H., Pan, J.J., Liu, D., Xu, G.L., Li, J.S., Ma, J.L., Jia, W.D., Yv, J.H., and Ge, Y.S. (2015b). Expression of Kindlin-1 in human hepatocellular carcinoma and its prognostic significance. Tumour Biol. *36*, 4235–4241.

Ma, Y.Q., Qin, J., Wu, C., and Plow, E.F. (2008). Kindlin-2 (Mig-2): a co-activator of beta3 integrins. J. Cell Biol. *181*, 439–446.

Mahawithitwong, P., Ohuchida, K., Ikenaga, N., Fujita, H., Zhao, M., Kozono, S., Shindo, K., Ohtsuka, T., Mizumoto, K., and Tanaka, M. (2013). Kindlin-2 expression in peritumoral stroma is associated with poor prognosis in pancreatic ductal adenocarcinoma. Pancreas *42*, 663–669.

Midde, K., Sun, N., Rohena, C., Joosen, L., Dhillon, H., and Ghosh, P. (2018). Single-cell imaging of metastatic potential of cancer cells. iScience *10*, 53–65.

Midde, K.K., Aznar, N., Laederich, M.B., Ma, G.S., Kunkel, M.T., Newton, A.C., and Ghosh, P. (2015). Multimodular biosensors reveal a novel platform for activation of G proteins by growth factor receptors. Proc. Natl. Acad. Sci. U S A *112*, E937–E946.

Minn, A.J., Gupta, G.P., Siegel, P.M., Bos, P.D., Shu, W., Giri, D.D., Viale, A., Olshen, A.B., Gerald, W.L., and Massague, J. (2005). Genes that mediate breast cancer metastasis to lung. Nature *436*, 518–524.

Montanez, E., Ussar, S., Schifferer, M., Bosl, M., Zent, R., Moser, M., and Fassler, R. (2008). Kindlin-2 controls bidirectional signaling of integrins. Genes Dev. *22*, 1325–1330.

Moore, D.T., Nygren, P., Jo, H., Boesze-Battaglia, K., Bennett, J.S., and Degrado, W.F. (2012). Affinity of talin-1 for the beta3-integrin cytosolic domain is modulated by its phospholipid bilayer environment. Proc. Natl. Acad. Sci. U S A *109*, 793–798.

Ren, X.D., Kiosses, W.B., and Schwartz, M.A. (1999). Regulation of the small GTP-binding protein Rho by cell adhesion and the cytoskeleton. EMBO J. *18*, 578–585.

Rognoni, E., Ruppert, R., and Fassler, R. (2016). The kindlin family: functions, signaling properties and implications for human disease. J. Cell Sci. *129*, 17–27.

Sahoo, D., Dill, D.L., Tibshirani, R., and Plevritis, S.K. (2007). Extracting binary signals from microarray time-course data. Nucleic Acids Res. *35*, 3705–3712.

Shen, Z., Ye, Y., Dong, L., Vainionpaa, S., Mustonen, H., Puolakkainen, P., and Wang, S. (2012). Kindlin-2: a novel adhesion protein related to tumor invasion, lymph node metastasis, and patient outcome in gastric cancer. Am. J. Surg. *203*, 222–229.

Shi, X., Ma, Y.Q., Tu, Y., Chen, K., Wu, S., Fukuda, K., Qin, J., Plow, E.F., and Wu, C. (2007). The MIG-2/integrin interaction strengthens cell-matrix adhesion and modulates cell motility. J. Biol. Chem. *282*, 20455–20466.

Sin, S., Bonin, F., Petit, V., Meseure, D., Lallemand, F., Bieche, I., Bellahcene, A., Castronovo, V., De Wever, O., Gespach, C., et al. (2011). Role of the focal adhesion protein kindlin-1 in breast cancer growth and lung metastasis. J. Natl. Cancer Inst. *103*, 1323–1337.

Smith, M.J., Hardy, W.R., Murphy, J.M., Jones, N., and Pawson, T. (2006). Screening for PTB domain binding partners and ligand specificity using proteome-derived NPXY peptide arrays. Mol. Cell. Biol. *26*, 8461–8474.

Spiess, M., Hernandez-Varas, P., Oddone, A., Olofsson, H., Blom, H., Waithe, D., Lock, J.G., Lakadamyali, M., and Stromblad, S. (2018). Active and inactive beta1 integrins segregate into distinct nanoclusters in focal adhesions. J. Cell Biol. *217*, 1929–1940.

Sun, Z., Lambacher, A., and Fassler, R. (2014). Nascent adhesions: from fluctuations to a hierarchical organization. Curr. Biol. *24*, R801–R803.

Talaat, S., Somji, S., Toni, C., Garrett, S.H., Zhou, X.D., Sens, M.A., and Sens, D.A. (2011). Kindlin-2 expression in arsenite- and cadmium-transformed bladder cancer cell lines and in archival specimens of human bladder cancer. Urology *77*, 1507.e1-7.

Theodosiou, M., Widmaier, M., Bottcher, R.T., Rognoni, E., Veelders, M., Bharadwaj, M., Lambacher, A., Austen, K., Muller, D.J., Zent, R., and Fassler, R. (2016). Kindlin-2 cooperates with talin to activate integrins and induces cell spreading by directly binding paxillin. Elife *5*, e10130.

Torgler, C.N., Narasimha, M., Knox, A.L., Zervas, C.G., Vernon, M.C., and Brown, N.H. (2004). Tensin stabilizes integrin adhesive contacts in Drosophila. Dev. Cell *6*, 357–369.

Vinogradova, O., Velyvis, A., Velyviene, A., Hu, B., Haas, T., Plow, E., and Qin, J. (2002). A structural mechanism of integrin alpha(IIb)beta(3) "inside-out" activation as regulated by its cytoplasmic face. Cell *110*, 587–597.

Volkmer, J.P., Sahoo, D., Chin, R.K., Ho, P.L., Tang, C., Kurtova, A.V., Willingham, S.B., Pazhanisamy, S.K., Contreras-Trujillo, H., Storm, T.A., et al. (2012). Three differentiation states risk-stratify bladder cancer into distinct subtypes. Proc. Natl. Acad. Sci. U S A *109*, 2078–2083.

Wang, Y., Klijn, J.G., Zhang, Y., Sieuwerts, A.M., Look, M.P., Yang, F., Talantov, D., Timmermans, M., Meijer-van Gelder, M.E., Yu, J., et al. (2005). Gene-expression profiles to predict distant metastasis of lymph-node-negative primary breast cancer. Lancet *365*, 671–679.

Wegener, K.L., Partridge, A.W., Han, J., Pickford, A.R., Liddington, R.C., Ginsberg, M.H., and Campbell, I.D. (2007). Structural basis of integrin activation by talin. Cell *128*, 171–182.

Winograd-Katz, S.E., Fassler, R., Geiger, B., and Legate, K.R. (2014). The integrin adhesome: from

genes and proteins to human disease. Nat. Rev. Mol. Cell Biol. *15*, 273–288.

Xu, Z., Chen, X., Zhi, H., Gao, J., Bialkowska, K., Byzova, T.V., Pluskota, E., White, G.C., 2nd, Liu, J., Plow, E.F., and Ma, Y.Q. (2014). Direct interaction of kindlin-3 with integrin alphallbbeta3 in platelets is required for supporting arterial thrombosis in mice. Arterioscler. Thromb. Vasc. Biol. *34*, 1961–1967.

Yan, M., Zhang, L., Wu, Y., Gao, L., Yang, W., Li, J., Chen, Y., and Jin, X. (2016). Increased expression of kindlin-2 is correlated with hematogenous metastasis and poor prognosis in patients with clear cell renal cell carcinoma. FEBS Open Bio. *6*, 660–665.

Ye, X., McLean, M.A., and Sligar, S.G. (2016). Phosphatidylinositol 4,5-bisphosphate modulates the affinity of talin-1 for phospholipid bilayers and activates its autoinhibited form. Biochemistry *55*, 5038–5048.

Zaidel-Bar, R., Cohen, M., Addadi, L., and Geiger, B. (2004). Hierarchical assembly of cell-matrix adhesion complexes. Biochem. Soc. Trans. *32*, 416–420.

Zaidel-Bar, R., Itzkovitz, S., Ma'ayan, A., Iyengar, R., and Geiger, B. (2007). Functional atlas of the integrin adhesome. Nat. Cell Biol. *9*, 858–867.

Zhan, J., Song, J., Wang, P., Chi, X., Wang, Y., Guo, Y., Fang, W., and Zhang, H. (2015). Kindlin-2 induced by TGF-beta signaling promotes pancreatic ductal adenocarcinoma progression through downregulation of transcriptional factor HOXB9. Cancer Lett. *361*, 75–85.

**iScience, Volume *23***

## Supplemental Information

# GIV●Kindlin Interaction Is Required for Kindlin-Mediated Integrin Recognition and Activation

**Cristina Rohena, Nicholas Kalogriopoulos, Navin Rajapakse, Suchismita Roy, Inmaculada Lopez-Sanchez, Jailal Ablack, Debashis Sahoo, and Pradipta Ghosh**

# SUPPLEMENTAL INFORMATION

## INVENTORY OF SUPPLEMENTARY MATERIALS

- **TRANSPARENT METHODS**
- **SUPPLEMENTARY FIGURES AND LEGENDS**
- **BIBLIOGRAPHY**

**TRANSPARENT METHODS**

- **Key Resource Table**
- **Contact for Reagent and Resource Sharing**
- **Experimental Model and Subject Details**
    - Cell Lines (Cos7, MDA-MB-231)
- **Method Details**
    - Cell culture
    - Whole Cell Immunofluorescence
    - Western Blotting
    - In Vitro Pulldown and Co-immunoprecipitation (CoIP)
    - Recombinant Protein Purification
    - Adhesion Assay
    - Transwell Invasion Assay
- **Quantification and Statistical Analysis**
    - Statistical Analysis
    - Replications
- **Data and Software Availability**

**Key Resource Table:**

| REAGENT or RESOURCE | SOURCE | IDENTIFIER |
|---|---|---|
| **ANTIBODIES** | | |
| **Rabbit monoclonal anti-pY1765 GIV** | Roche Spring Biosciences | 06974937001 Clone SP158 |
| **Rabbit polyclonal anti-GIV CT** | Santa Cruz Biotechnology | N/A |
| **Rabbit polyclonal anti-Gαi3 (C-10)** | Santa Cruz Biotechnology | N/A |
| **Rabbit polyclonal anti-β-tubulin** | Santa Cruz Biotechnology | sc-9104 |
| **Mouse monoclonal anti-GAPDH** | Santa Cruz Biotechnology | sc-365062 |
| **Mouse monoclonal anti-HIS** | GenScript | A00186-100 |
| **Mouse monoclonal anti-GST** | GenScript | A00865 |
| **Mouse monoclonal anti-α-tubulin** | Santa Cruz Biotechnology | sc-5286 |
| **Mouse monoclonal anti-pFAK** | BD Biosciences | 611722 |

| | | |
|---|---|---|
| **Mouse monoclonal anti-paxillin** | BD Biosciences | 610051 |
| **Mouse monoclonal anti-vinculin** | Sigma-Aldrich | V9131 |
| **Rabbit polyclonal anti-paxillin** | Santa Cruz Biotechnology | SC-5574 |
| **Mouse monoclonal anti-kindlin2** | EMD Millipore | MAB2617 |
| **Rat anti-active β1 integrin** | BD Pharmingen | 9EG7 |
| **Mouse monoclonal anti-β1 integrin** | Abcam | Ab30394 |
| **Goat anti-Rabbit IgG (680)** | LI-COR Biosciences | 926-68071 |
| **Goat anti-Rabbit IgG, Alexa Fluor 594 conjugated** | ThermoFisher Scientific | A11072 |
| **Goat anti-Rabbit IgG, Alexa Fluor 647 conjugated** | ThermoFisher Scientific | A27040 |
| **Goat anti-Mouse IgG (800)** | LI-COR Biosciences | 926-32210 |
| **Goat anti-Mouse IgG, Alexa Fluor 488 conjugated** | Thermo Fisher Scientific | A11017 |
| **Biological Samples and Cell Lines** | | |
| **Cos7** | ATCC | CRL-1651 |
| **MDA-MB-231** | ATCC | HTB-26 |
| **CHEMICALS, RECOMBINANT PROTEINS, AND PLASMIDS** | | |
| **DAPI (4',6-Diamidino-2-Phenylindole, Dilactate)** | Thermo Fisher Scientific | D3571 |
| **Collagen I** | BD Biosciences | 354249 |
| **Poly-D-lysine** | Millipore Sigma | A-003-E |
| **Mirus TranIT LT1** | Mirus Bio LLC | MIR2300 |
| **G418** | Cellgro | A-1720 |
| **Puromycin** | Life Technologies | A1113803 |
| **Biocoat Matrigel Invasion Inserts** | Corning | 354480 |
| **Paraformaldehyde 16%** | Electron Microscopy Biosciences | 15710 |
| **Phalloidin 594** | Thermo Fisher Scientific | A12381 |
| **Prolong Gold** | Thermo Fisher Scientific | P10144 |
| **Prolong Glass** | Thermo Fisher Scientific | P36980 |
| **pGEX-4T-GIV-CT-WT (a.a. 1623-1870)** | (Garcia-Marcos et al., 2009) | N/A |
| **pET-28b-GIV-CT-WT (a.a. 1660-1870)** | (Garcia-Marcos et al., 2009) | N/A |
| **pET-28b-GIV-CT-PGxA(a.a. 1660-1870)** | This paper | N/A |
| **CMV14-p3X FLAG-GIV WT (full length)** | This paper | N/A |
| **pGEX4T-Kindlin C term ; [GST-mFERM2 (571-680)]** | (Montanez et al., 2008) | N/A |

| | | |
|---|---|---|
| **pGEX-4T1-Kindlin2 C-term QW/AA [GST-mFERM2 (571-680), Q614A/W615A]** | (Montanez et al., 2008) | N/A |
| **GST-mFERM2(564-680)** | This paper | N/A |
| **GST-mFERM2(564-680) QW/AA [Q614A/W615A]** | This paper | N/A |
| **6xHis-SUMO-Kindlin2Δ** | (Li et al., 2017) | N/A |
| **CMV14-p3X FLAG-GIV PGxA (full length)** | This paper | N/A |
| **pGEX-4T1-Tensin3-SH2-PTB** | (Qian et al., 2009) | N/A |
| **pGEX-4T1-Tensin3 -SH2** | (Qian et al., 2009) | N/A |
| **pGEX4T-Integrin beta 3** | (Montanez et al., 2008) | N/A |
| **pGEX4T-Integrin beta 1** | (Montanez et al., 2008) | N/A |
| **pGEX-6P-GST- Talin-F3 domain** | (Ye et al., 2010) | N/A |
| **Kindlin2 siRNA** | Santa Cruz Biotechnology; (Yang et al., 2016) | sc-106786 |
| **SOFTWARE** | | |
| **ImageJ** | National Institute of Health | https://imagej.net/Welcome |
| **Prism** | GraphPad | https://www.graphpad.com/scientific-software/prism/ |
| **LAS-X** | Leica | www.leica-microsystems.com/products/microscope-software/p/leica-las-x-ls |
| **Molsoft ICM v3.8-6** | Molsoft LLC | http://www.molsoft.com/index.html |

## Methods

### Plasmid constructs and protein expression

Cloning of GIV-CT (aa 1660–1870) into pET28b (His-GIV CT) was described previously (Garcia-Marcos et al., 2012) GST-K2F3, GST-β1-CT and GST-β3-CT plasmids were generously obtained from Reinhardt Fassler (Max Planck Institute, Germany). GST-Tensin3 plasmid was generously obtained from Douglas Lowy, the GST-Talin plasmids and His-β1-CT plasmids were obtained from Mark H. Ginsberg (UC San Diego), and the 6xHis-SUMO-Kindlin2Δ construct (Li et al., 2017) was generously provided by Prof. Cong Yu (.Southern University of Science and Technology, Shenzhen, China). For mammalian expression, RNA interference–resistant (shRNA rest) GIV was cloned into p3XFLAG-CMVTM-14 plasmid (GIV-FLAG) as described previously (Garcia-Marcos et al., 2009) GIV-FLAG and His-GIV-CT mutants (F1742A) were generated by site-directed mutagenesis using a QuikChange

kit (Stratagene, CA, USA) and specific primers (sequence available upon request) as per the manufacturer's protocols (Garcia-Marcos et al., 2009, Lin et al., 2011) Primer sequences are available upon request. shRNA 3–untranslated region for GIV (GIV shRNA: CCGGGCTTTCATT-ACCAGCTCTGAACTCGAGTTCAGAGCTGGTAATGAAAGCTTTTTTG) was cloned into pLKO.1 (TRCN0000130452) or control vector TRC1.5-pLKO.1-puro. His-GIV-CT fusion construct was expressed in E. coli strain BL21 (DE3) and purified as described previously (Garcia-Marcos et al., 2009, Ghosh et al., 2008). Briefly, bacterial cultures were induced overnight at 25°C with 1 mM isopropyl β-d-1-thiogalactopyranoside (IPTG). Pelleted bacteria from 1 l of culture were resuspended in 10 ml of His lysis buffer (50 mM NaH2PO4, pH 7.4, 300 mM NaCl, 10 mM imidazole, 1% [vol:vol] Triton X-100, 2X protease inhibitor cocktail [Complete EDTA-free, Roche Diagnostics, CA, USA]). After sonication (3 × 30 s), lysates were centrifuged at 12,000 × g at 4°C for 20 min. Solubilized proteins were affinity purified on HisPur Cobalt Resin (Pierce, IL, USA). Proteins were eluted, dialyzed overnight against PBS, and stored at −80°C.

GST-mFERM2(564-680) (encoding for the F3 domain of mouse Kindlin2, Uniprot Q8CIB5, C-terminal to GST and the SDLVPRGSPEL linker, as part of a pGX4T-1 expression vector) was generated from the GST-mFERM2(571-680) generously shared by Reinhard Faessler (Max Planck Institute, Germany) (Montanez et al., 2008) Similarly, GST-mFERM2(564-680) Q614A/W615A was made from GST-mFERM2(571-680) Q614A/W615A. The constructs were generated using standard site directed mutagenesis protocol. The PCR products were amplified using the forward primer: TCTCTGCCTGAGTTCGGCATCACACACTTCATTGCGAGG and reverse primer: GATGCCGAACTCAGGCAGAGACAATTCCGGGGATCCACG, using Pfu Turbo (Agilent, CA, USA), digested by *Dpn I* (NEB, UK), transformed into XL10 (Gold) competent cells, and grown on agar plates with 50 mg/mL Carbenicillin. All the aforementioned constructs were checked by sequencing with PGEX universal primer (Genewiz, USA).

***Recombinant Protein Purification***

Both GST and His-tagged proteins were expressed in E. coli stain BL21 (DE3) and purified as previously described (ref). Briefly, cultures were induced using 1mM IPTG overnight at 25°C. Cells were then pelleted and resuspended in either GST lysis buffer (25 mM Tris-HCl, pH 7.5, 20 mM NaCl, 1 mM EDTA, 20% (vol/vol) glycerol, 1% (vol/vol) Triton X-100, 2×protease inhibitor cocktail) or His lysis buffer (50 mM $NaH_2PO_4$ (pH 7.4),

300 mM NaCl, 10 mM imidazole, 1% (vol/vol) Triton X-100, 2X protease inhibitor cocktail). Cells were lysed by sonication, and lysates were cleared by centrifugation at 12,000 X g at 4°C for 30 mins. Supernatant was then affinity purified using glutathione-Sepharose 4B beads (GE Healthcare) or HisPur Cobalt Resin (Thermo Fisher Scientific), followed by elution, overnight dialysis in PBS, and then storage at -80°C.

For expressing and purifying His-Kindlin-2, 6xHis-SUMO-Kindlin2Δ plasmid was transformed into Rosetta cells for protein expression. For large scale purification, 2 L of secondary culture was induced at 25°C overnight using 0.2 mM IPTG. Cell pellet was resuspended in Resuspension Buffer (RB) consisting of 50mM phosphate buffer pH 7.4, 300mM NaCl, 5 mM bME, 5 mM imidazole, DNAse, and 1 tablet of protease inhibitor cocktail (Roche, added fresh before use). The suspension was sonicated (Branson Digital sonicator) with 18% pulse with 30 second time on and off for five minutes each until the protein suspension was clear, after which Triton X-100 was added to 0.1%. The suspension was centrifuged at 13,000 rcf for 45min. The supernatant was collected and incubated with Talon resin (Takara, Japan) for 2h at 4°C. The resin was then washed with RB + 50 mM imidazole and eluted with RB + 200 mM imidazole. The eluted protein was loaded into a size exclusion column (Superdex 200 Increase 10/300, GE Healthcare, USA) with SEC buffer as HEPES pH 7.5, 100 mM NaCl, 1mM MgCl2, 1 mM DTT. The fractions were collected, pooled, spin-concentrated using Amicon® Ultra (Sigma, MO, USA) with a 30 kDa MW cutoff, flash-frozen in small aliquots, and stored at -80 for further use.

***In Vitro Pulldown and Co-immunoprecipitation (Co-IP)***

Purified GST-tagged proteins from E. coli were immobilized onto glutathione-Sepharose beads and incubated with binding buffer (50 mM Tris-HCl pH 7.4, 100 mM NaCl, 0.4% (v:v) Nonidet P-40, 10 mM MgCl2, 5 mM EDTA, 2 mM DTT, 1X Complete protease inhibitor) for 60min at room temperature. For GST-pulldown assays with recombinant proteins, the proteins were diluted in binding buffer and incubated with immobilized GST-proteins for 90min at room temperature. For binding with cell lysates, cells were lysed in cell lysis buffer (20 mM HEPES pH 7.2, 5 mM Mg-acetate, 125 mM K-acetate, 0.4% Triton X-100, 1 mM DTT, 500 µM sodium orthovanadate, phosphatase inhibitor cocktail (Sigma-Aldrich, MO, USA) and protease inhibitor cocktail (Roche Life Science)) using a 28G syringe, followed by centrifugation at 10,000Xg for 10min. Cleared supernatant was then used in binding reaction with immobilized GST-proteins for 4 hours at 4°C. After binding, bound complexes were washed four times with 1 ml phosphate wash buffer (4.3 mM Na2HPO4, 1.4 mM KH2PO4, pH 7.4, 137 mM NaCl, 2.7

mM KCl, 0.1% (v:v) Tween 20, 10 mM MgCl2, 5 mM EDTA, 2 mM DTT, 0.5 mM sodium orthovanadate). Bound proteins were then eluted through boiling at 100°C in Laemmli buffer (BIORAD, CA, USA). For experiments using Kindlin-2 constructs (both GST and His), the bound proteins were eluted at 37°C for 10 min.

***Cell culture, transfection, lysis, and quantitative immunoblotting***

Cos7, HeLa and MDA-MB-231 cells were obtained from American Type Culture Collection (ATCC). Transfection, lysis, and immunoblotting were carried out exactly as described before (Aznar et al., 2016, Lopez-Sanchez et al., 2015) Cells were transfected using Mirus LT1 following the manufacturers' protocols. For assays involving serum starvation, serum concentration was reduced to 0% FBS overnight.

Whole-cell lysates were prepared after washing cells with cold PBS before resuspending and boiling them in sample buffer. Lysates used as a source of proteins in pull-down assays were prepared by resuspending cells in lysis buffer (20 mM HEPES, pH 7.2, 5 mM Mg acetate, 125 mM K acetate, 0.4% Triton X-100, and 1 mM dithiothreitol supplemented with sodium orthovanadate [500 μM], phosphatase [Sigma-Aldrich, MO, USA], and protease [Roche, USA] inhibitor cocktails), after which they were passed through a 28-gauge needle at 4°C and cleared (10,000 × g for 10 min) before use in subsequent experiments.

For immunoblotting, protein samples were separated by SDS-PAGE and transferred to polyvinylidene fluoride membranes (Millipore Sigma, MO, USA). Membranes were blocked with PBS supplemented with 5% nonfat milk (or with 5% BSA when probing for phosphorylated proteins) before incubation with primary antibodies. In some instances, the samples were separated on a 12% SDS PAGE and transferred to a nitrocellulose membrane (Bio-Rad, CA, USA) using TransBlot-Turbo (Bio-Rad, CA, USA). The membrane was stained with Ponceau S to visualize baits, then washed and blocked with PBS with 0.1% Tween (PBS-T) and 0.5% BSA overnight at 4°C. Infrared imaging with two-color detection and quantification were performed using a Li-Cor Odyssey imaging system. Dilution of primary antibodies used were as follows: anti–GIV-CT, 1:500; anti-Gαi3, 1:333; anti-β tubulin, 1:1000; anti-β1 integrin, 1:250; and anti–His, 1:500. All blots were visualized using LI-COR Odyssey imager, and band analysis was performed with Image Studio™ Lite 5.2 (LI-COR Biosciences, NE, USA). Figures were assembled for presentation using Photoshop (Adobe, San Jose, CA, USA) and Illustrator (Adobe, San Jose, CA, USA) software.

***Generation of stable cell lines***

shRNA control and shRNA GIV MDA-MB-231, stable cell lines using Mission RNAi technology (Sigma-Aldrich, MO, USA) were generated by lentiviral transduction followed by selection with puromycin (2.5 μg/ml) a described previously (Midde et al., 2018). Depletion of endogenous GIV was confirmed by immunoblotting with GIV-CT rabbit antibody. Lentiviral packaging was performed in HEK293T cells by co-transfecting the shRNA constructs with psPAX2 and pMD2G plasmids (4:3:1 ratio, respectively), using Mirus LT1. The medium was changed after 24 h, and virus-containing medium was collected after 36–48 h and centrifuged and filtered through a 0.45-μm filter. psPAX2 and pMD2G plasmids were a generous gift from Christopher K. Glass (University of California, San Diego, La Jolla, CA). shRNA GIV MDA-MB-231 stable cell lines expressing p3xFLAG-CMV-14-GIV (GIV-3xFLAG) WT and PGxA constructs were selected as previously described (Aznar et al., 2016) with the neomycin analogue G418 at 800 μg/ml. Expression of various GIV constructs were confirmed to be similar to levels of endogenous GIV in shRNA control cells by immuno-blotting with GIV-CT antibodies.

***Whole-cell confocal immunofluorescence***

Cells were fixed at room temperature with 3% PFA in PBS for 15 min, treated with 0.1 M glycine for 10 min, and subsequently permeabilized for 1 h (0.2% Triton X-100 in PBS) and blocked in PBS containing 1% bovine serum albumin (BSA) and 0.1% Triton X-100 as described previously (Lopez-Sanchez et al., 2014). Primary and secondary antibodies where incubated for 1h at room temperature in blocking buffer. ProLong Gold or Prolong Glass (Life Technologies, USA) was used as mounting medium. Dilutions of antibodies used were as follows: phosphotyrosine (pY)-1764-GIV, 1:300; vinculin, 1:400; paxillin, 1:200; integrin-β1, 1:400; phalloidin, 1:1000; phospho-FAK, 1:100; kindlin-2, 1:150; conformational specific antibody integrin-β1, 1:400; DAPI, 1:2000; and secondary goat anti-rabbit (488), goat anti-mouse (594), and goat-anti-mouse or rabbit (647) Alexa-conjugated antibodies, 1:500. Images were acquired at room temperature with a Leica TCS SPE-II with DMI4000 microscope equipped with a Leica Hamamatsu 9100-02 camera and the LAS AF SPE software (Leica, Germany) using a 63× oil-immersion objective using 488-, 561-, 635-, and 405-nm laser lines for excitation. The settings were optimized, and the final images scanned with line averaging of three scans. Images were further processed using Lightning deconvolution in the Leica LAS-X (Leica Microsystems, Germany) software package. Quantification of focal adhesions was carried out using the particle analyzer application on ImageJ (NIH, MD,

USA) exactly as outlined previously (Horzum et al., 2015 blue right-pointing triangle). All images were processed using ImageJ software and assembled for presentation using Photoshop and Illustrator software. Images shown are representative of 90–95% cells that were evaluated across three independent experiments.

***Molecular modeling***

A NMR-resolved structure of DLC1(peptide) bound to the PTB domain of tensin [(Chen et al., 2012) PDB 2loz] and a structure of β1-integrin-bound dimerized 6xHis-SUMO-Kindlin2Δ [(Li et al., 2017) PDB 5xq0] were used as docking templates to model β1-integrin-bound Kindlin-2. Modeling was carried out using Molsoft (see STAR materials Table).

***Super Resolution* Stimulated emission depletion (STED*) microscopy***

This was performed using a Leica TCS SP8 Confocal microscope equipped with a white light laser tunable to excitations between 470 and 670nm. Cells were plated on collagen-coated coverslips and allowed to adhere for 30 min. They were then fixed with 4% PFA and stained with antibodies against kindlin2 (1:100), pYGIV (1:100) or Paxillin (1:100) followed by secondary antibody incubation (AlexaFluor 488 and AlexaFluor 647 1:500). Coverslips were then mounted on Prolong Glass and allowed to cure for 5 days before imaging. Images were acquired using the HyD detectors with the tunable white light laser set to the corresponding Alexa 488 and Alexa 647 nm excitation and emission wavelengths. Because of the combination of fluorophores used depletion lasers of 592 nm were used for the 488 channel and depletion laser of 775 nm used for the 647 nm channel. A 100x oil objective was used to acquire all images. Once images were acquired, they were deconvolved using LAS-X software and then processed using ImageJ. All images were further processed in ImageJ using the 3D surface plot plugin and line scans were done to generate RGB plots.

***Transwell invasion assay***

Cell invasion was assessed using Biocoat Matrigel (Corning, NY, USA) inserts with 8-μm pores in 24-well plates. Cells were detached using trypsin/EDTA and resuspended in DMEM supplemented with 0.4% FBS. A total of 5 × 105 cells was loaded in the upper well in a volume of 300 μl, and the lower well was filled with 750 μl of DMEM with 10% FBS. The plates were incubated at 37°C for 24h before removing the remaining cell suspension. The

invasion insert was placed in a clean well containing 4% PFA for 1 h at room temperature, stained with crystal violet for 1 h, and washed three times in PBS. Cells on the upper side of the filters were removed with cotton-tipped swabs, and the number of migrated cells on the bottom side of the filter was counted in five randomly chosen fields at 200× magnification and averaged. All experiments were performed in triplicate, and each experiment was repeated at least three times.

***Adhesion Assay***

12-well plates were coated with collagen, rinsed with PBS, and then blocked with 0.5% BSA for 1h at 37°C. Cells were harvested with trypsin/EDTA, seeded in the wells at 2 × 104 cells/well in 1,000 µl of DMEM with 0.4% FBS, and allowed to adhere for 30min at 37°C. Nonadherent cells were removed by gentle washing twice with PBS, and attached cells were fixed in 4% PFA for 15 min and then stained with 2.3% crystal violet (Sigma-Aldrich, MO, USA) for 10min. Cells were extensively washed, air dried, and then the cells imaged and counted using ImageJ. All experiments were performed in triplicate, and each experiment was repeated at least three times.

***Analysis of gene expression data***

Gene expression data from three different cohorts of patients with breast cancers (Minn et al., 2005, Bos et al., 2009, Wang et al., 2005) were collected from the National Center for Biotechnology Information (NCBI) Gene Expression Omnibus (GEO) website (Barrett, T. et al. 2005; Edgar et al., 2002). The dataset was prepared by pooling data from GSE2034, GSE2603 and GSE12276 and normalizing them together using Robust Multi-chip Average (RMA) algorithm. Patient survival data were carefully annotated for Kaplan-Meier analysis. To derive optimal cut-off values of gene expression levels, they are ordered from low to high and a rising step function was computed to define a threshold by StepMiner algorithm (Sahoo et al., 2007). Gene expression values were converted to high and low levels based on the StepMiner threshold. A noise margin of +/- 0.5 was used around the StepMiner threshold to provide relaxed estimates of the high/low values. A noise margin of +/- 0.5 around StepMiner threshold was used to soften or harden the actual threshold. Time-dependent survival probabilities are estimated with the Kaplan-Meier method (Kaplan EL, 1958) and compared using the log-rank test (Peto et al., 1977). Cox proportional-hazards regression models and life-tables (Cox, 1972) were used to test the statistical interaction between two different genes based on their association with survival outcome. High and

low expression patterns for focal genes such as GIV (CCDC88A), K2 (FERMT2) and ITGB1 were compared individually using Kaplan-Meier analyses in R statistical software (R version 3.4.4 2018-03-15). Statistical interaction (synergistic effects) between the focal adhesion genes GIV (CCDC88A), K2 (FERMT2), ITGB1, TLN1 (talin 1), TNS1 (tensin 1), TENC1 (TNS2, tensin 2), TNS3 (tensin 3), TNS4 (tensin 4), PXN (paxillin), and VCL (vinculin) were measured using interaction terms in Cox proportional hazards regression model on the above pooled breast cancer dataset with survival data. For example, coefficient of interaction terms was computed from Cox regression model for CCDC88A and FERMT2 as follows:

$$\mathrm{h(t)} = \mathrm{h_0(t)exp(a1 * CCDC88A + a2 * FERMT2 + a3 * CCDC88A * FERMT2)}$$

where $\mathrm{h(t)}$ is the hazard rate at time $\mathrm{t}$ for an individual; $\mathrm{a1, a2, and\ a3}$ are the regression coefficients; $\mathrm{h_0(t)}$ is the baseline hazard; two indicator variables $\mathrm{CCDC88A}$ and $\mathrm{FERMT2}$ (high expression = 1 else 0) that had only additive or interactive effects; $\mathrm{a3}$ is the coefficient of interaction terms.

**Data analysis and other methods**

All experiments were repeated at least three times, and results were presented either as one representative experiment or as average ± SD. Statistical significance was assessed with the Student's t test. Statistical significance between datasets with three or more experimental groups was determined using one-way analysis of variance (ANOVA) including a Tukey's test for multiple comparisons. *$p < 0.05$, **$p < 0.01$, ***$p < 0.001$, ****$p < 0.0001$.

## SUPPLEMENTARY FIGURES AND LEGENDS

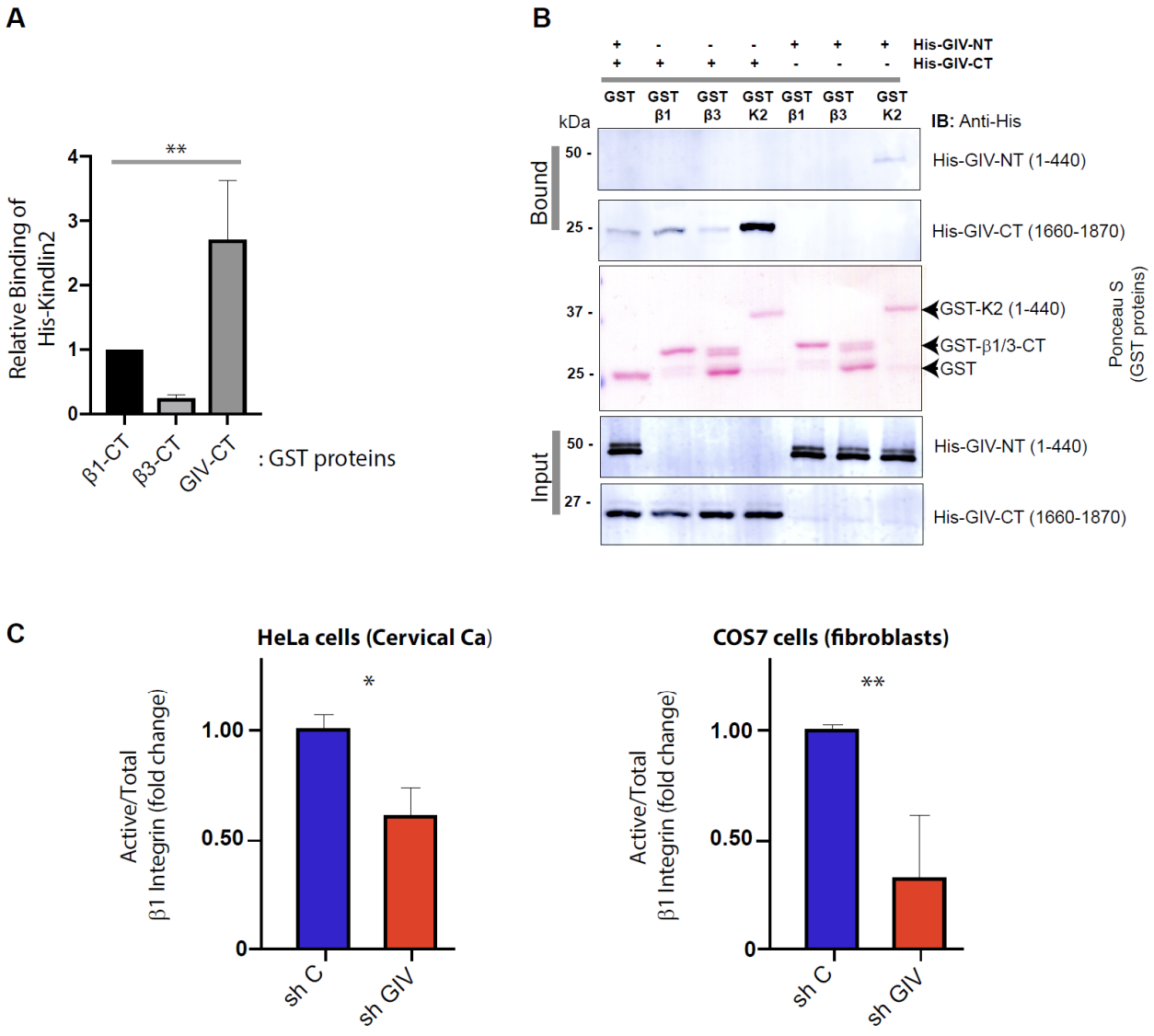


**Figure S1 [Related to Figure 1]**:

**The C-terminus, but not the terminus of GIV binds directly and strongly to Kindlin-2, and to a much weaker degree to β1-integrin tail**.

- **A.** Bar graphs display the relative binding of His-Kindlin 2 to various GST proteins in **Fig 1C**. Error bar = S.E.M (n = 3); **p=<0.01.
- **B.** GST pulldown assays were carried out using His-tagged GIV--CT or NT proteins (~ 3 μg) and GST-tagged β1-integrin tails and Kindlin protein immobilized on glutathione beads. Equal loading of input (lower panels) and bound (upper panels) proteins were visualized by immunoblotting with anti-His antibody. GST proteins were visualized using Ponceau S staining.
- **C.** Bar graphs display the fold change in the ratio of total and active β1-integrins, as determined by FACS studies conducted on control (sh C) and GIV-depleted (sh GIV) cells. Data are represented as mean ± SEM (n = 3); **p=<0.01.

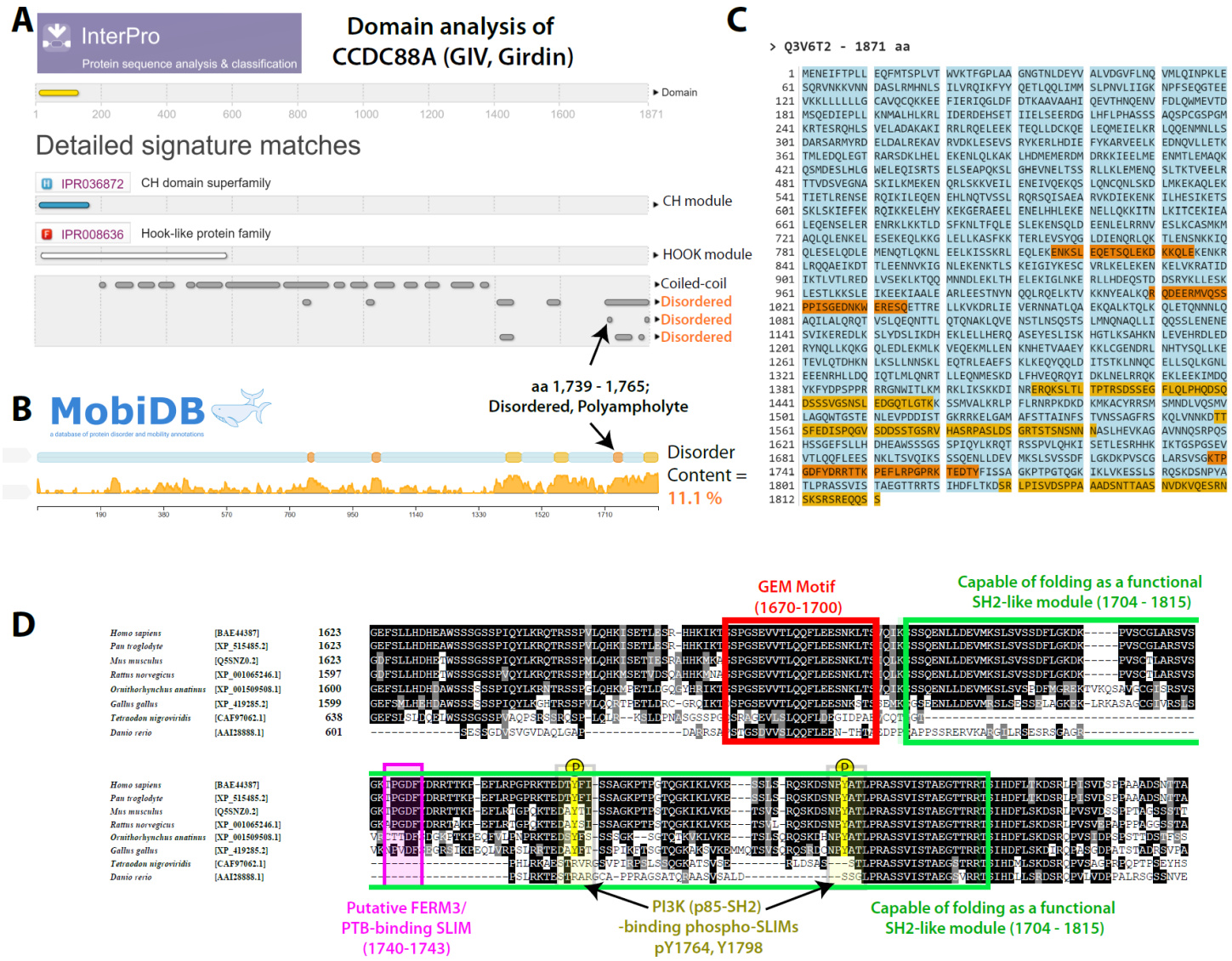


**Figure S2 [Related to Figure 2]**:

**GIV's C-terminal ~ 300-400 amino acid stretch is largely disordered, and aa 1739 – 1765 is predicted to have the highest disorderliness. A.** GIV's sequence was analyzed for structural modularity using InterPro [https://www.ebi.ac.uk/interpro/], a web based program that provides functional analysis of proteins by classifying them into families and predicting domains and important sites by finding matches against a number of member databases into a single searchable resource. Analysis showed the previously known and validated presence of N-terminal coiled coil and Hook domains. The C-terminus is predicted to have disordered segments, which was also confirmed by a secondary web-based applications, MobiDB [http://mobidb.bio.unipd.it/], which represents the disorder content as 2D plots (**B**). The intensity of orange color denotes the degree of disorderliness. **C**. Sequence of GIV with highlighted stretches of disorderliness shows highest disorderliness in the stretch aa 1739-1765, within which the putative FERM3-PTB binding sequence PGxF is located. **D**. Sequence alignment of GIV's C-terminus showing a complete catalog of previously validated short linear motifs (SLIMS) and modules; the position of the newly identified FERM3-PTB binding SLIM (aa 1740-1743) is shown in pink. Because it is located within GIV's SH2-like module, it is unlikely that GIV would bind RTKs and Kindlin (or other PTB modules) simultaneously. Because multiple phosphosites flank this SLIM, it is likely that binding of GIV to PTB modules are regulated by post-translational modifications.

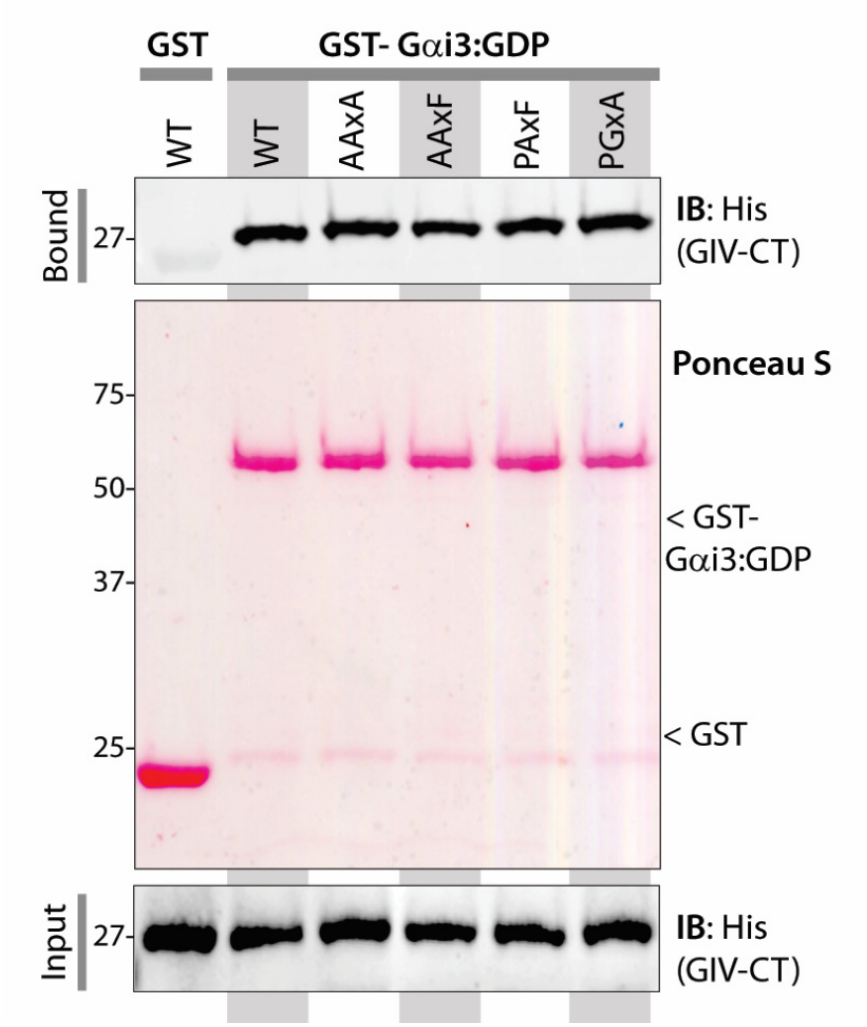


**Figure S3 [Related to Figure 2]**:

**Mutations that impair GIV•K2 interaction do not perturb the GIV•Gαi interaction.** GST pulldown assays were performed using of His-GIV-CT WT or various mutants targeting its PGxF sequence and GST-Gαi3 (pre-loaded with GDP). Equal loading of GST proteins was confirmed by Ponceau S staining.

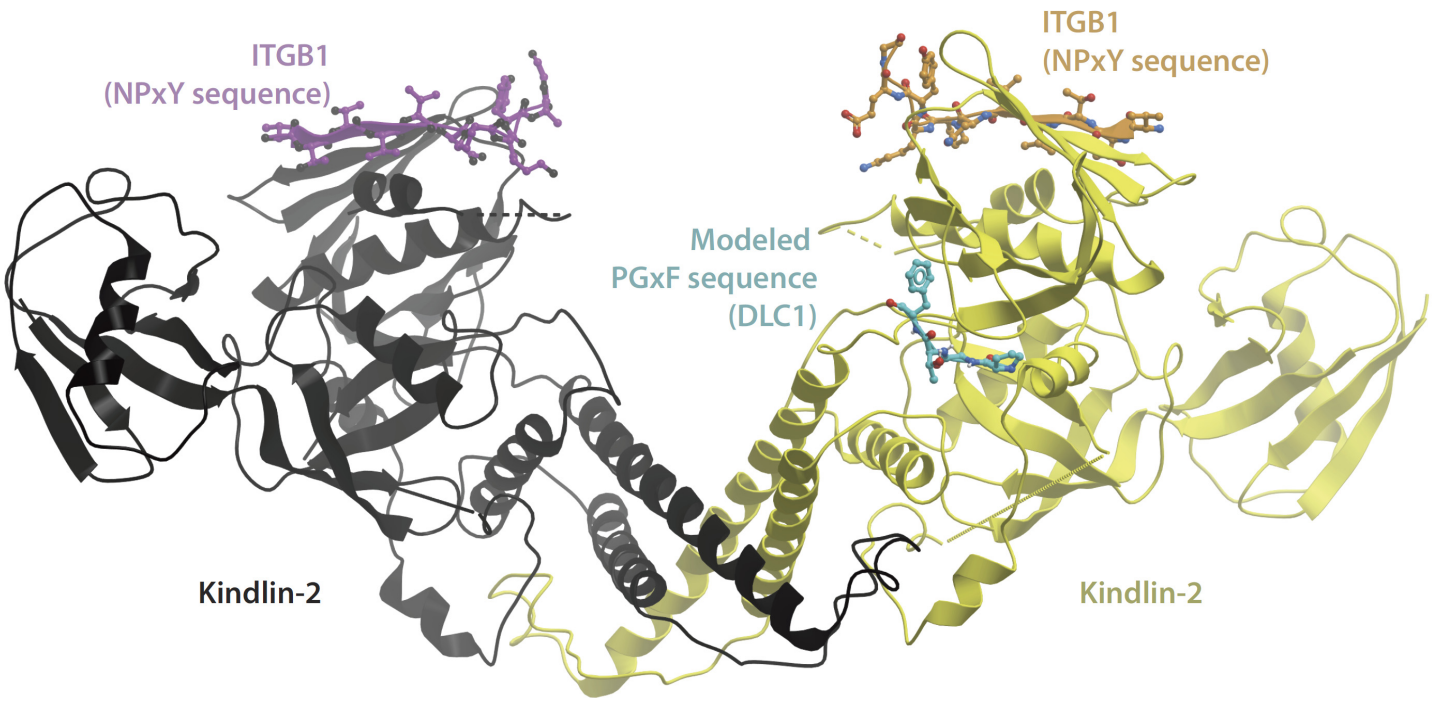


**Figure S4 [Related to Figure 2]**:

**The proposed GIV-PGxF sequence binding surface is accessible in dimerized Kindlin-2.** Figure shows the solved structure of K2 dimers (black and yellow) bound to ITGB1 tail (magenta and orange). The proposed interface with PGxF motif (teal blue) is shown on one of the monomeric units (yellow) when engaged as a dimer. This model was created using the solved structures of ITGB1-bound K2 (PDB:5XQ0) and DLC1(PGxF)•tensin complex structure (PDB:2LOZ).

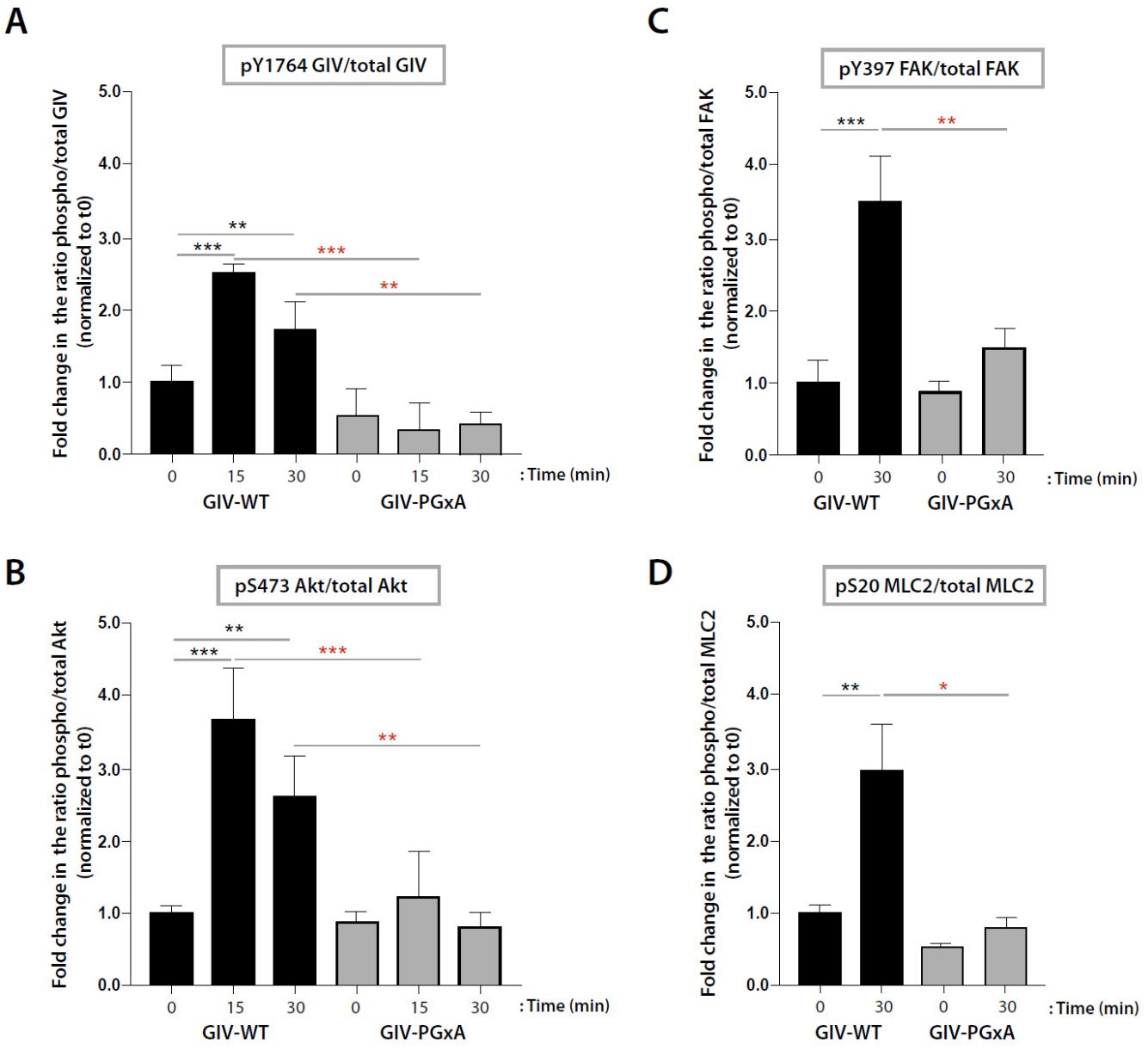


**Figure S5 [Related to Figure 4]**:

**Mutations that impair GIV•K2 interaction suppress major signaling pathways previously shown to be triggered downstream of Integrin β1.** Bar graphs display quantification of 3-4 independent experiments measuring the ratio of phospho/total GIV (**A**), Akt (**B**), FAK (**C**) and MLC2 (**D**). Data are represented as mean ± SEM. *p < 0.05, **p < 0.01, ***p < 0.001. See **Fig 4J-L** for representative blots.

**SUPPLEMENTARY REFERENCES:**


AZNAR, N., PATEL, A., ROHENA, C. C., DUNKEL, Y., JOOSEN, L. P., TAUPIN, V., KUFAREVA, I., FARQUHAR, M. G. & GHOSH, P. 2016. AMP-activated protein kinase fortifies epithelial tight junctions during energetic stress via its effector GIV/Girdin. *Elife,* 5.

BOS, P. D., ZHANG, X. H., NADAL, C., SHU, W., GOMIS, R. R., NGUYEN, D. X., MINN, A. J., VAN DE VIJVER, M. J., GERALD, W. L., FOEKENS, J. A. & MASSAGUE, J. 2009. Genes that mediate breast cancer metastasis to the brain. *Nature,* 459**,** 1005-9.

CHEN, L., LIU, C., KO, F. C., XU, N., NG, I. O., YAM, J. W. & ZHU, G. 2012. Solution structure of the phosphotyrosine binding (PTB) domain of human tensin2 protein in complex with deleted in liver cancer 1 (DLC1) peptide reveals a novel peptide binding mode. *J Biol Chem,* 287**,** 26104-14.

COX, D. R. 1972. Regression models and life tables (with discussion). *J R Statist Soc,* B**,** 187-220.

GARCIA-MARCOS, M., GHOSH, P. & FARQUHAR, M. G. 2009. GIV is a nonreceptor GEF for G alpha i with a unique motif that regulates Akt signaling. *Proc Natl Acad Sci U S A,* 106**,** 3178-83.

GARCIA-MARCOS, M., KIETRSUNTHORN, P. S., PAVLOVA, Y., ADIA, M. A., GHOSH, P. & FARQUHAR, M. G. 2012. Functional characterization of the guanine nucleotide exchange factor (GEF) motif of GIV protein reveals a threshold effect in signaling. *Proc Natl Acad Sci U S A,* 109**,** 1961-6.

GHOSH, P., GARCIA-MARCOS, M., BORNHEIMER, S. J. & FARQUHAR, M. G. 2008. Activation of Galphai3 triggers cell migration via regulation of GIV. *J Cell Biol,* 182**,** 381-93.

KAPLAN EL, M. P. 1958. Nonparametric estimation from incomplete observations. *J Am Stat Assoc,* 53**,** 457-481.

LI, H., DENG, Y., SUN, K., YANG, H., LIU, J., WANG, M., ZHANG, Z., LIN, J., WU, C., WEI, Z. & YU, C. 2017. Structural basis of kindlin-mediated integrin recognition and activation. *Proc Natl Acad Sci U S A,* 114**,** 9349-9354.

LIN, C., EAR, J., PAVLOVA, Y., MITTAL, Y., KUFAREVA, I., GHASSEMIAN, M., ABAGYAN, R., GARCIA-MARCOS, M. & GHOSH, P. 2011. Tyrosine phosphorylation of the Galpha-interacting protein GIV promotes activation of phosphoinositide 3-kinase during cell migration. *Sci Signal,* 4**,** ra64.

LOPEZ-SANCHEZ, I., DUNKEL, Y., ROH, Y. S., MITTAL, Y., DE MINICIS, S., MURANYI, A., SINGH, S., SHANMUGAM, K., AROONSAKOOL, N., MURRAY, F., HO, S. B., SEKI, E., BRENNER, D. A. & GHOSH, P. 2014. GIV/Girdin is a central hub for profibrogenic signalling networks during liver fibrosis. *Nat Commun,* 5**,** 4451.

LOPEZ-SANCHEZ, I., MA, G. S., PEDRAM, S., KALOGRIOPOULOS, N. & GHOSH, P. 2015. GIV/girdin binds exocyst subunit-Exo70 and regulates exocytosis of GLUT4 storage vesicles. *Biochem Biophys Res Commun,* 468**,** 287-93.

MIDDE, K., SUN, N., ROHENA, C., JOOSEN, L., DHILLON, H. & GHOSH, P. 2018. Single-Cell Imaging of Metastatic Potential of Cancer Cells. *iScience,* 10**,** 53-65.

MINN, A. J., GUPTA, G. P., SIEGEL, P. M., BOS, P. D., SHU, W., GIRI, D. D., VIALE, A., OLSHEN, A. B., GERALD, W. L. & MASSAGUE, J. 2005. Genes that mediate breast cancer metastasis to lung. *Nature,* 436**,** 518-24.

MONTANEZ, E., USSAR, S., SCHIFFERER, M., BOSL, M., ZENT, R., MOSER, M. & FASSLER, R. 2008. Kindlin-2 controls bidirectional signaling of integrins. *Genes Dev,* 22**,** 1325-30.

PETO, R., PIKE, M. C., ARMITAGE, P., BRESLOW, N. E., COX, D. R., HOWARD, S. V., MANTEL, N., MCPHERSON, K., PETO, J. & SMITH, P. G. 1977. Design and analysis of randomized clinical trials requiring prolonged observation of each patient. II. analysis and examples. *Br J Cancer,* 35**,** 1-39.

QIAN, X., LI, G., VASS, W. C., PAPAGEORGE, A., WALKER, R. C., ASNAGHI, L., STEINBACH, P. J., TOSATO, G., HUNTER, K. & LOWY, D. R. 2009. The Tensin-3 protein, including its SH2 domain, is phosphorylated by Src and contributes to tumorigenesis and metastasis. *Cancer Cell,* 16**,** 246-58.

SAHOO, D., DILL, D. L., TIBSHIRANI, R. & PLEVRITIS, S. K. 2007. Extracting binary signals from microarray time-course data. *Nucleic Acids Res,* 35**,** 3705-12.

WANG, Y., KLIJN, J. G., ZHANG, Y., SIEUWERTS, A. M., LOOK, M. P., YANG, F., TALANTOV, D., TIMMERMANS, M., MEIJER-VAN GELDER, M. E., YU, J., JATKOE, T., BERNS, E. M., ATKINS, D. & FOEKENS, J. A. 2005. Gene-expression profiles to predict distant metastasis of lymph-node-negative primary breast cancer. *Lancet,* 365**,** 671-9.

YANG, J. R., PAN, T. J., YANG, H., WANG, T., LIU, W., LIU, B. & QIAN, W. H. 2016. Kindlin-2 promotes invasiveness of prostate cancer cells via NF-kappaB-dependent upregulation of matrix metalloproteinases. *Gene,* 576**,** 571-6.

YE, F., HU, G., TAYLOR, D., RATNIKOV, B., BOBKOV, A. A., MCLEAN, M. A., SLIGAR, S. G., TAYLOR, K. A. & GINSBERG, M. H. 2010. Recreation of the terminal events in physiological integrin activation. *J Cell Biol,* 188**,** 157-73.